

Chapter 3 Simulation and Discussion

In this chapter, we will bring up a series of research focusing on both waveguide properties and 2-D photonic crystals devices. Four subjects have been discussed in the following text, including energy hopping behavior in the PhCs waveguides, WDM design using point defect, dual wavelength demultiplexing and bi-direction (BIDI) front-end. Many related and additional points have also been analyzed.

3-1 Energy hopping in the photonic crystal waveguides

In order to take well advantage of the photonic crystal waveguides in photonic circuits, we have to make a complete understanding about the physical properties of the EM waves propagating through them. The theoretical and numerical investigation of energy flow (Poynting vector) in PhCs waveguides made of line defects has been reported [21]. Here we do another different discussion about the energy flow in detail.

3-1.1 Line-defect photonic crystal waveguides

By introducing the line defect into a perfect photonic crystal, we can obtain a waveguide which guides light with ultra-low loss in certain frequencies. The line defect, such as reduced or enlarged rod (hole), can be created by inserting miscellaneous defect which breaks the symmetry of perfect photonic crystals, even make a slightly move to the rod (hole). Table 3-1 makes an exhibition of many kinds of line-defect photonic crystal waveguides. We need to mention here only the dispersion relation and the energy distribution of each case.

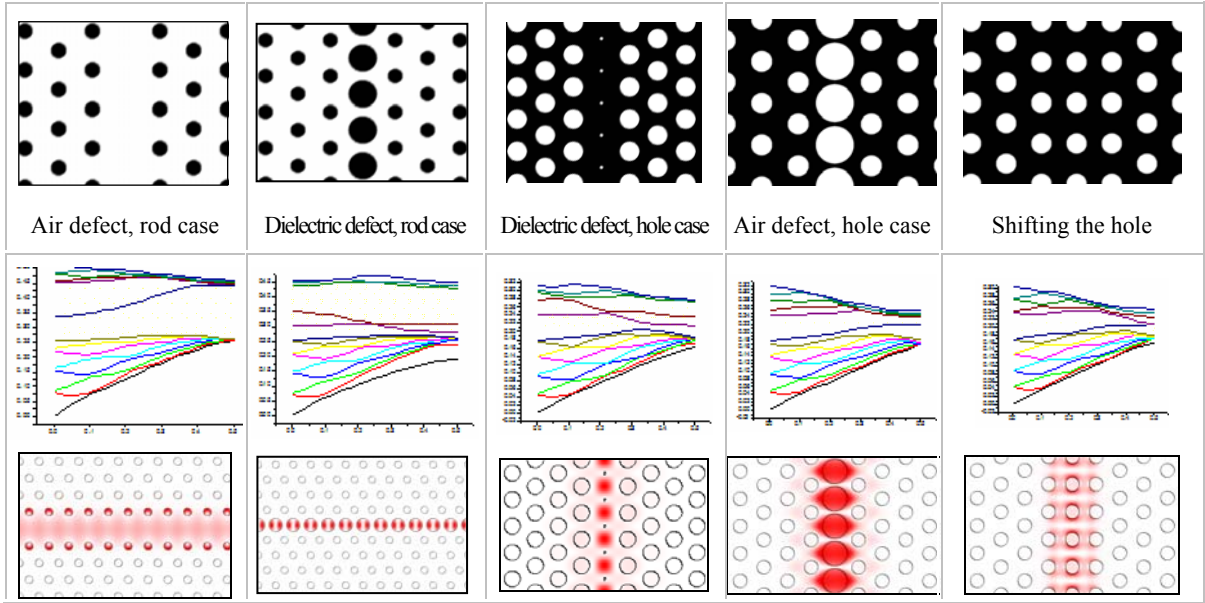


Table 3-1. The dispersion relation and energy distribution of some different PhCs waveguides.

Our photonic crystal structure is a two-dimensional triangular lattice with lattice constant Λ in the background of air. The diameter and dielectric constant of rod is 0.4Λ and 12. A line defect is introduced by reducing the radius of the rods, denoted as R_d . Both dispersion relations in TM-polarization of void rod ($R_d = 0 \Lambda$) and reduced rod ($R_d = 0.1 \Lambda$) can be calculated by using plane-wave expansion method, along Γ -X direction is shown in Fig. 3-1.

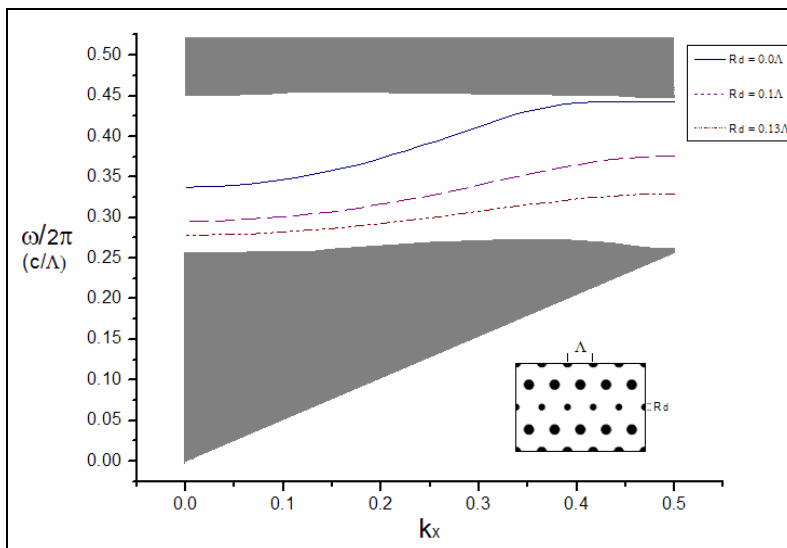


Fig. 3-1. The defect mode drops from the upper band while R_d is decreasing gradually.

3-1.2 The energy flow and field localization

Fig. 3-2 and Fig. 3-3 are the distribution of the time-averaged energy density and poynting vector (S) in the case of $R_d = 0.1 \Lambda$ with $k_x = 0.4$ near the zone boundary. In Fig. 3-2(a), we can observe the EM wave is highly concentrated in the defect rods ($R_d = 0.1 \Lambda$) of the waveguides, and the profiles at these different k_x -points ($k_x = 0.4, 0.27$ and 0.1) are shown in Fig. 3-2(b). As the diagrams indicate, the energy density (U) in the defect rods is almost two orders of magnitude stronger than that in the air region. The energy confined in the defect rod takes 50 % of total energy (within entire supercell), although the defect rod has only 5 % of the area of one unit cell only. Furthermore, the same phenomenon happens in the poynting vector. The profile of the poynting vector in x-component (S_x) along the center of the waveguide at these different k_x -points is shown in Fig. 3-3(b). The same observation applies to the case of void rod (Fig. 3-4).

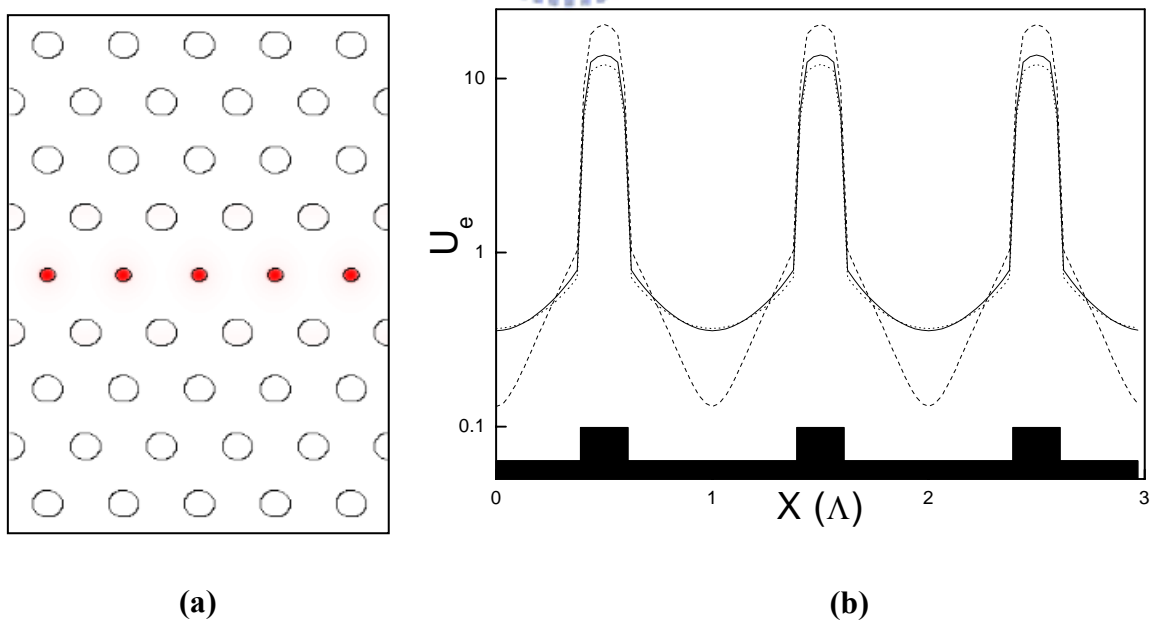


Fig. 3-2. (a) Distribution of the time-averaged energy density at $k_x = 0.4$. (b) Energy density in three different k_x points (where the shadowed region is our defect rods index profiles). The dish, solid and dot lines indicate the $k_x = 0.4, 0.27$ and 0.1 .

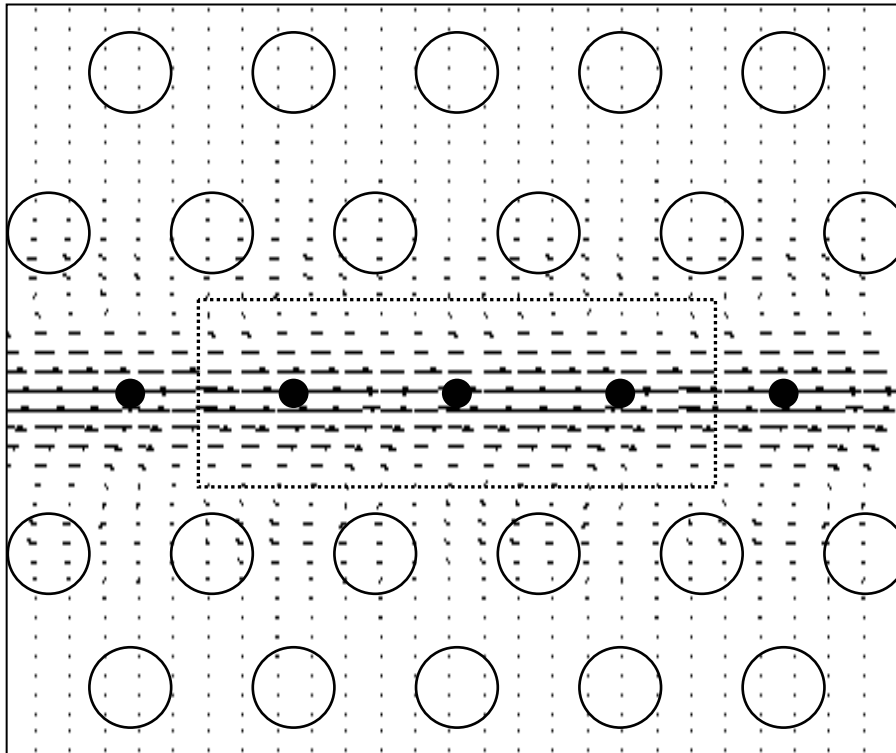
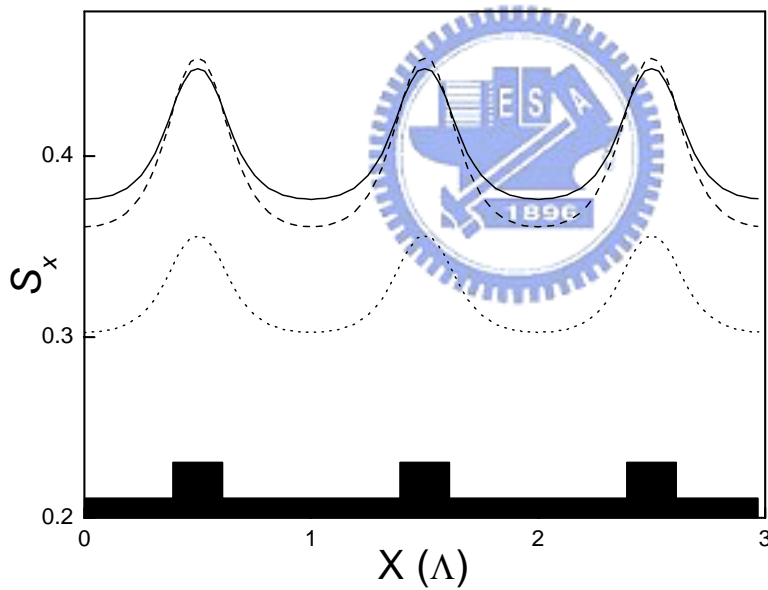


Fig. 3-3.

(a) Poynting vector at $k_x = 0.4$, the energy mainly flows parallel to the waveguide.



(b) Poynting vector in x component (Where the dish, solid and dot lines indicate the $k_x = 0.4$, 0.27 and 0.1).

We can recognize from the diagrams above that the localization of energy is more concentrative while near the band edge.

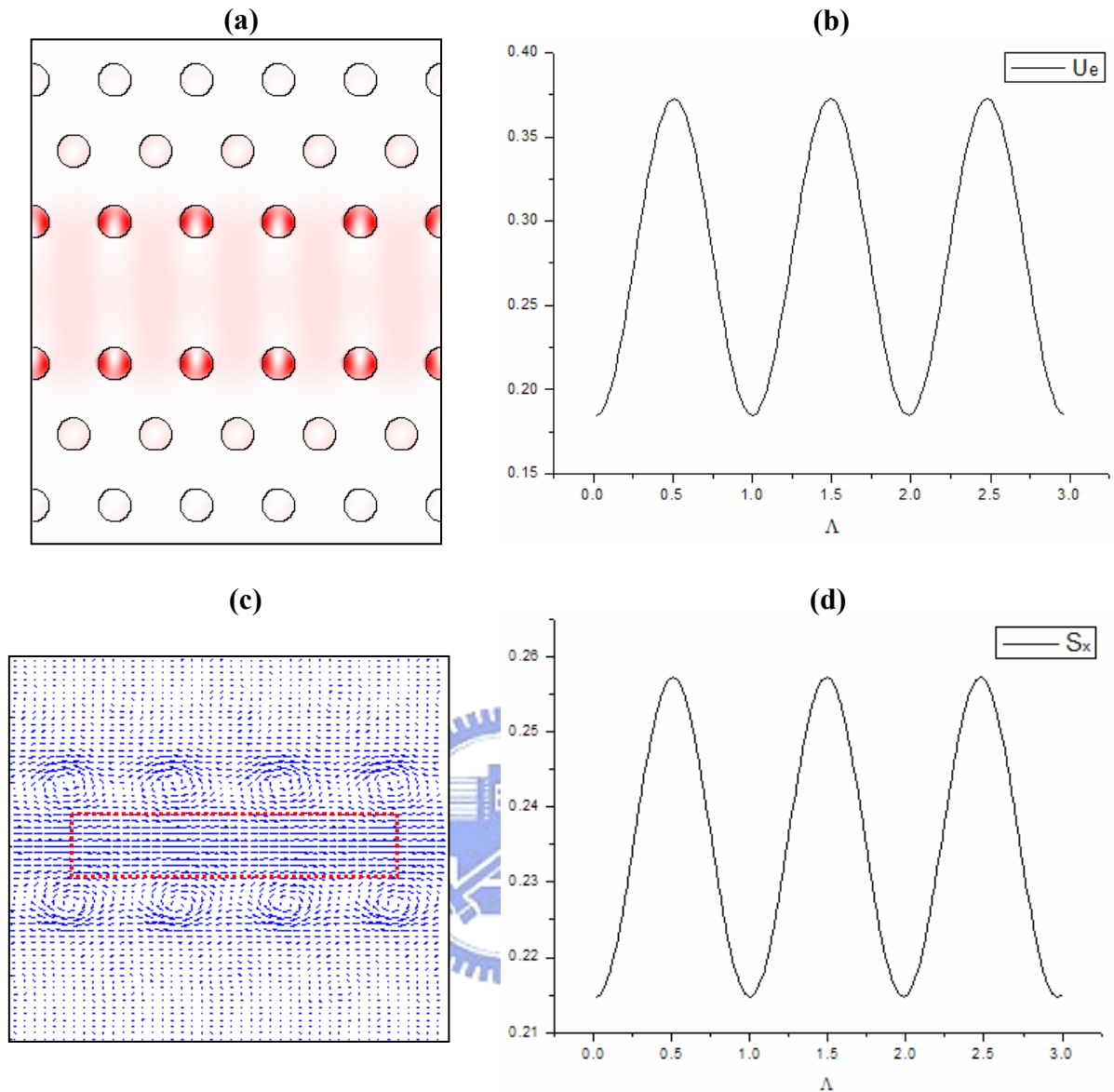


Fig. 3-4. Void rod case in $k_x = 0.4$ point. (a) Time-averaged energy density. (b) Energy profile. (c) Energy flow (poynting vector, S). (d) The x-component of S in the central waveguide.

3-1.3 Group velocity and tunneling mechanism

Group velocity signifies the speed of the energy flow. It can be calculated by either the ratio of the spatial average of S_x to that of U in a unit cell and $\frac{\partial \omega}{\partial k}$ of the dispersion relation.

Curve fitting between them agrees quite well (Fig. 3-5). As $k_x = 0.4$ in Fig. 3-6(a), the EM

wave propagates in the defect rods at the speed only 2 % of light speed (c) in vacuum. It indicates that the EM wave is localized in the defect rods, which acts like a cavity, and the localized waves couple to their neighbors due to the overlapping of their evanescent waves. For $k_x = 0.25$ and 0.1 , in the reduced rods the energies still are well confined and propagate at very low speed ($0.03c$). The energy densities are lower than the former case ($k_x = 0.4$), indicating there are more overlapping of the modes. The speed is higher than c ($2.76c$) between the defect rods, it explains the transition of the energy between the rods is a tunneling mechanism, not uniform flow or pure wave propagation. The similar situation can also be found in some special void rods cases.

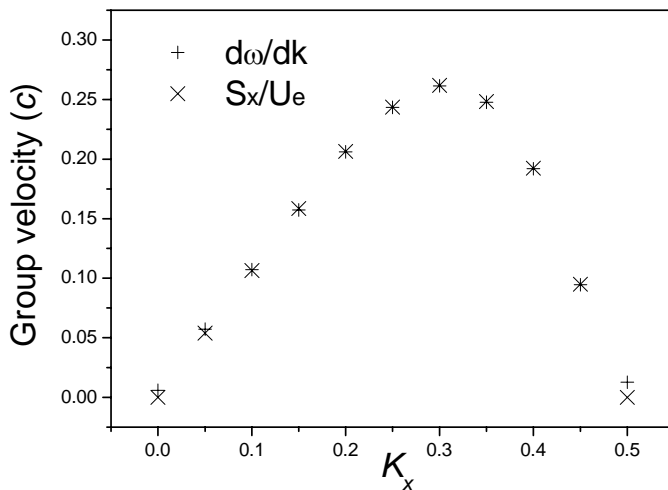


Fig. 3-5.

The $\frac{\partial\omega}{\partial k}$ and $\frac{\langle S_x \rangle}{\langle U_e \rangle}$ match pretty well.

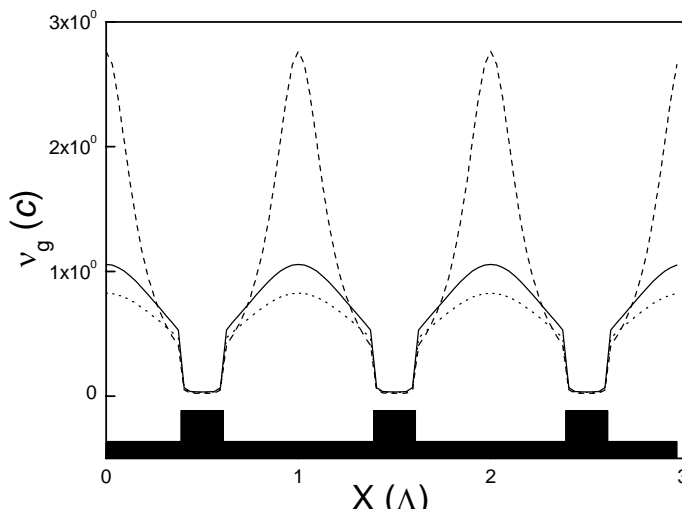


Fig. 3-6. (a)

The group velocity between the defect rods can reach $2.76c$, on the contrary, the EM wave propagates inside the defect rod at the speed only $0.02c$ (long dwelling time). These indicate that the PhCs waveguide acts like a cavity. (Where the dish, solid and dot lines indicate the $k_x = 0.4, 0.27$ and 0.1).

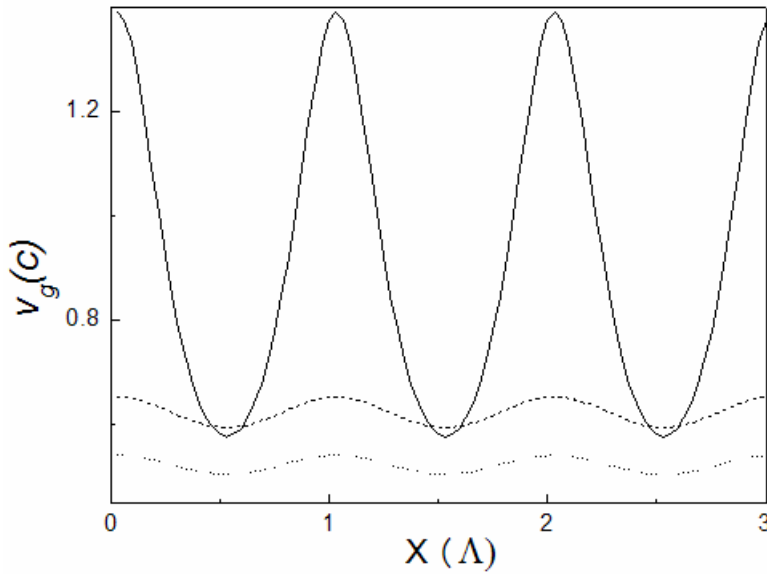


Fig. 3-6. (b)

The same situation of group velocity in void rods case. The v_g can reach to $1.39c$ while near the band edge. It also indicates that a void rods PCW also acts like a CCW even its hopping mechanism is not so obvious as reduced rods case. (Where the solid, dash and dot lines indicate the $k_x = 0.4, 0.27$ and 0.1).

For reasons we mentioned above, the PhCs waveguide can be regarded as a coupled-cavity waveguide (CCW), in which the energy hops from a cavity to the neighbor one [33].



3-1.4 Coupled cavity waveguides and tight-binding approximation

A point defect, acts as an optical resonator (cavity), can be created by introducing a single defect into a photonic crystal that locally trap photons with certain frequencies inside the defect volume (Fig. 3-7(a)). A coupled-cavity waveguide (CCW) is formed by placing several point defects side by side with a periodicity of Λ (Fig. 3-7(b)). Fig. 3-8 illustrates that the guiding mechanism of CCW is due to evanescent coupling of the single defect modes. The overlap of the waveguides of the defect modes is large enough to provide energy tunneling of the EM waves along the tightly confined cavity modes. Its experimental results are also proved and published in the early time [34-36]. Base on this, the propagation of wave through a coupled-cavity waveguide (CCW) is exactly the classic wave analog of the tight-binding (TB) method in solid-state physics [34-36].

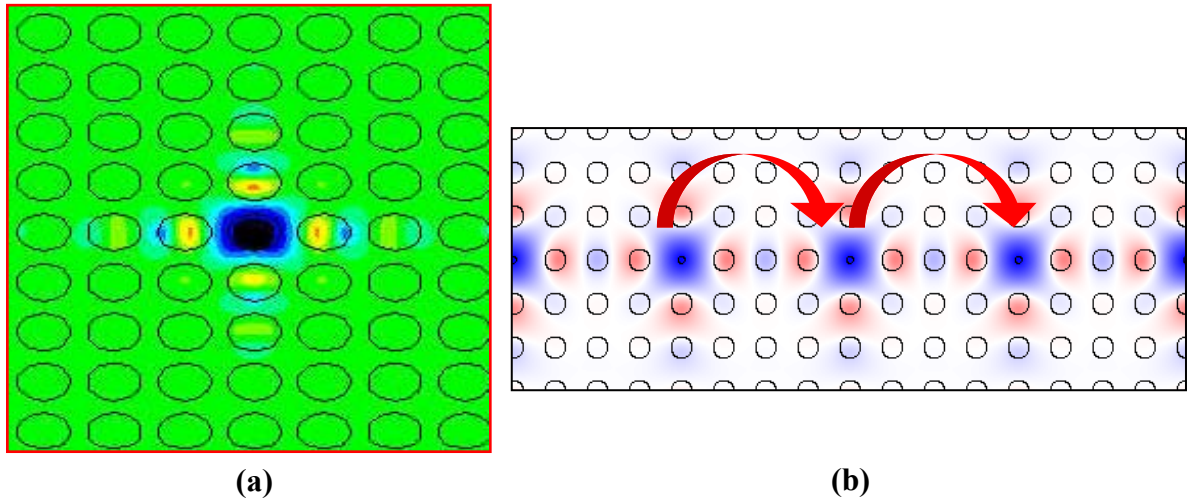


Fig. 3-7. (a) A single point defect, in which the photon in resonance frequency is trapped inside the point defect. (b) A diagram of coupled cavity waveguide (CCW).

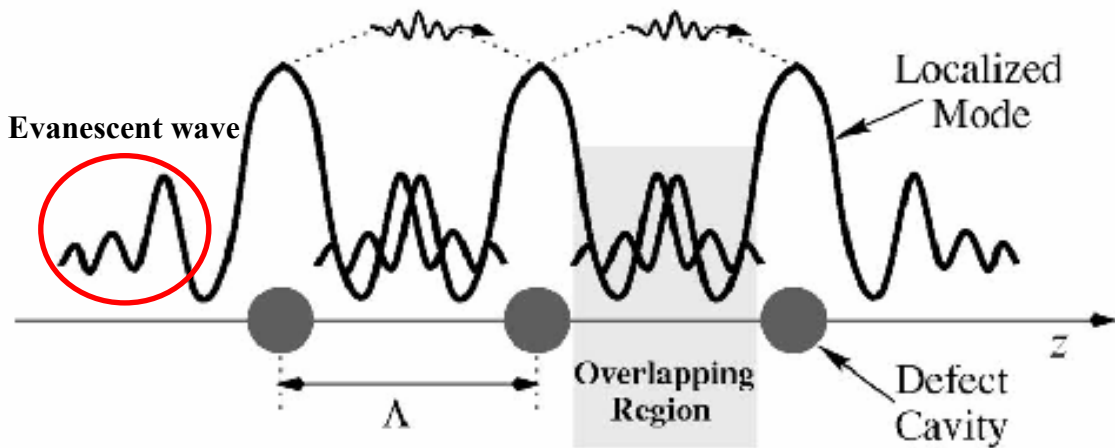


Fig. 3-8. Schematics of propagation of photons by the coupled evanescent defect modes.

The dispersion relation of CCW can be further described using TB approximation (refer to section 2-4) by

$$\omega = \Omega + \alpha \cos(k_x \Lambda) + \beta \cos(2k_x \Lambda) + \gamma \cos(3k_x \Lambda) + \delta \cos(4k_x \Lambda) + \dots, \quad (3.1)$$

where Ω is the resonant frequency of a single cavity and α , β , γ and δ are the TB parameters determined from splitting of several coupled cavities or the width of defect band. Equation (3.1) states the different strength of evanescent waves coupling to the neighbors. The farther the coupling, the more terms are required to get a well curve fitting of defect bands. Curve fitting of our two different defect bands in Fig. 3-1 ($R_d = 0 \Lambda$ and 0.1Λ) have accomplished (Fig. 3-9(a) and 3-9(b)). Each fitting parameters in different orders are shown in Table 3-2 below. Such ideal fitting curves support our suggestion that the rods in the line defect act as cavities.

Rd	Line type	Ω	α	β	γ	δ	Error
0.0Λ	Dot	0.39458	-0.0599	0.00209	0.00151	-0.00058	7.27E-09
	Solid	0.39501	-0.06076	0.00284	0.00089	--	1.15E-07
0.1Λ	Dot	0.33153	-0.03945	0.0039	-0.00036	-0.00006	8.88E-10
	Solid	0.33119	-0.03884	0.00343	--	--	3.32E-08

Table 3-2. Curve fitting parameters at both void and reduced rod cases.

From the case of $R_d = 0 \Lambda$ in Fig. 3-1, we notice the defect mode was compressed by the upper band edge in the region of $k_x \approx 0.36$ to 0.5 . According to this, the data above $k_x = 0.36$ was neglected to avoid the error of curve fitting parameters. As demonstrates in Table 3-2, the gradual decrease of TB parameters ($\alpha \dots \delta$) is a result of fewer coupling between the further neighboring rods. We found there is significant even of the next farther neighboring rods for the reduced rod case, due to more confined field as shown in Fig. 3.2(a). However, the field distribution of single defect extends over a distance at least 3 lattice constants for the void rod case.

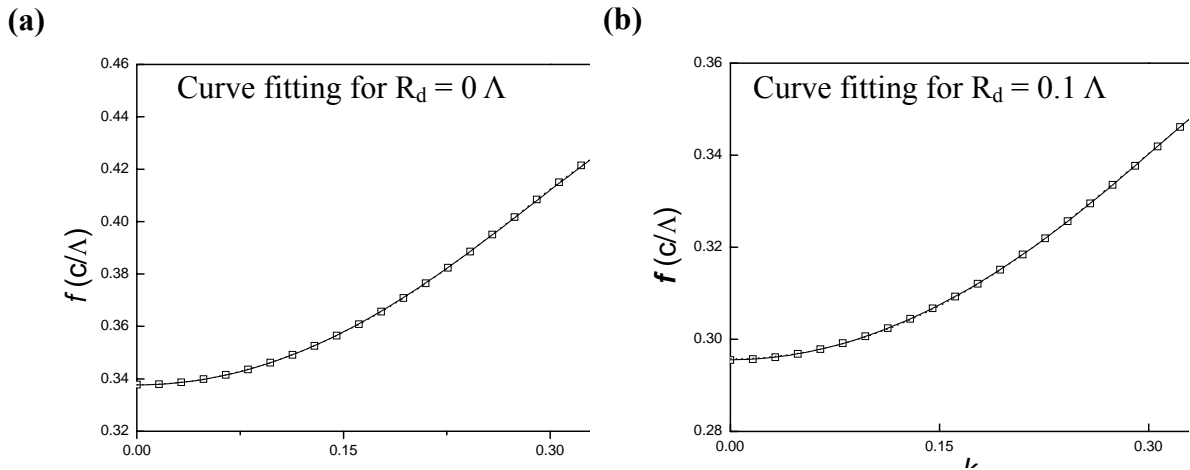


Fig. 3-9. (a)(b) The fitting results of our void and reduced rod defect bands. Where the squares are our 2 defect bands which are calculated by MPB.


3-1.5 Summary

In this section, we have reported the properties of energy transit within the photonic crystal waveguides in 2D triangular-lattice photonic crystal of different defects, void rods and reduced rods. The dispersion relation of both cases can be well fitted by TB approximation, but there are significant differences like photons transit and the coupling behavior with the neighbors in these two types of waveguides. For the case of reduced rods, in the defect rods the energy density is extremely high while the group velocity is extremely low compared with that in the vicinal air. The energy transit can be described by hopping due to the overlapping of evanescent waves in quantum mechanics.

3-2 Photonic crystal WDM for application of point defect

Wavelength division multiplexing (WDM) plays an essential role in optical communication. It allows network operators to more efficiently utilize bandwidth by aggregating separate wavelengths or channels onto a single optical fiber and offers an attractive solution to increasing the bandwidth of fiber network without disturbing the existing employed fiber trunk system. In order to develop the photonic integrated circuits (PICs) in the future, the size of devices must be substantially reduced. Using photonic crystal devices may be a most possible solution to achieve integrated circuit. In this section, we will make a skeleton design of photonic crystal WDM using point defect.

3-2.1 Photonic crystal directional coupler



We start with a device called photonic crystal directional coupler. When two PhC waveguides are brought in close vicinity of each other they will form what is known as a directional coupler, shown in Fig. 3-10. Under suitable conditions, the electromagnetic waves launched into one of the PhC waveguide can completely couple to the nearby waveguide. Once the waves have crossed over, the waves will couple back into the first waveguide so that the power is exchanged continuously. Under a precise calculation, two lightwaves can be split resulting from their own coupling length. According to this, a PhC WDM might be possibly fabricated. Unfortunately, based on the severe standard of extinction ratio in optical communication (20 dB is required in normal), by using a usual directional coupler is pretty hard to achieve that performance. The Fig. 3-11 helps to catch on to this argument.

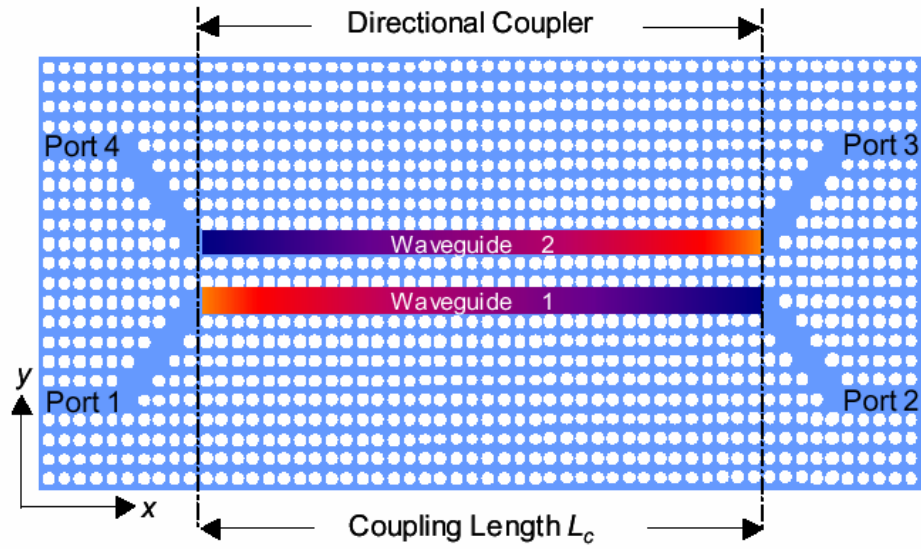


Fig. 3-10. Photonic crystal directional coupler consisting of two closely coupled PhC waveguides.

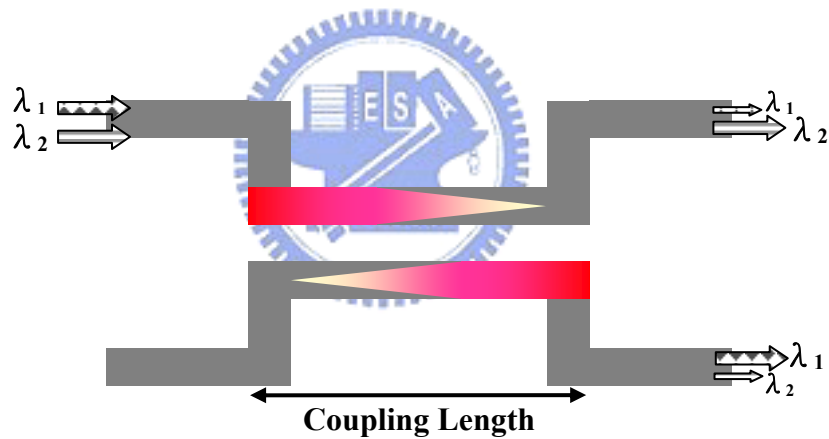


Fig. 3-11. A diagram of the fault in power ratio in usual PhC directional coupler.

3-2.2 The PhC point defect and design ideal

After our exposition in section one, we decided to discard the directional coupler and look for another solution. The behavior of point defect may be useful to us. As we known, certain of few wavelengths can be trapped within a point defect and be the steady resonance states. One can simply control the resonance wavelength by only modulating the size of the

point defect. Now we have a good tool to do the PhC WDM design.

Point defect can be treated as a filter instead of a cavity. By pumping a PhC point defect with multi-wavelength, only a narrow bandwidth of frequency can successfully exist and resonate inside. If we combine two point defects to form a “short” coupled-cavity waveguide (CCW). A PhC filter is easily realized. Fig. 3-12 shows the defect mode of CCW (also called as slow-light band) and the work function about PhC filter.

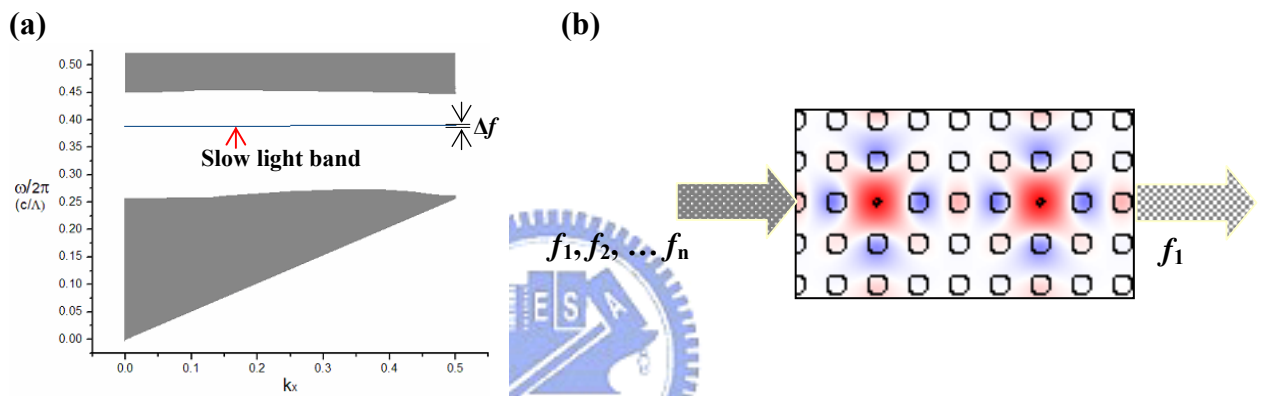
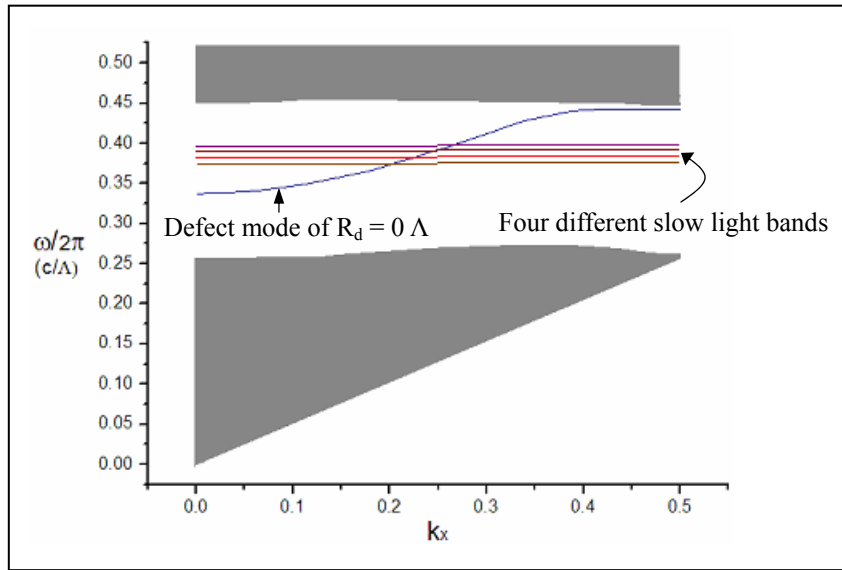
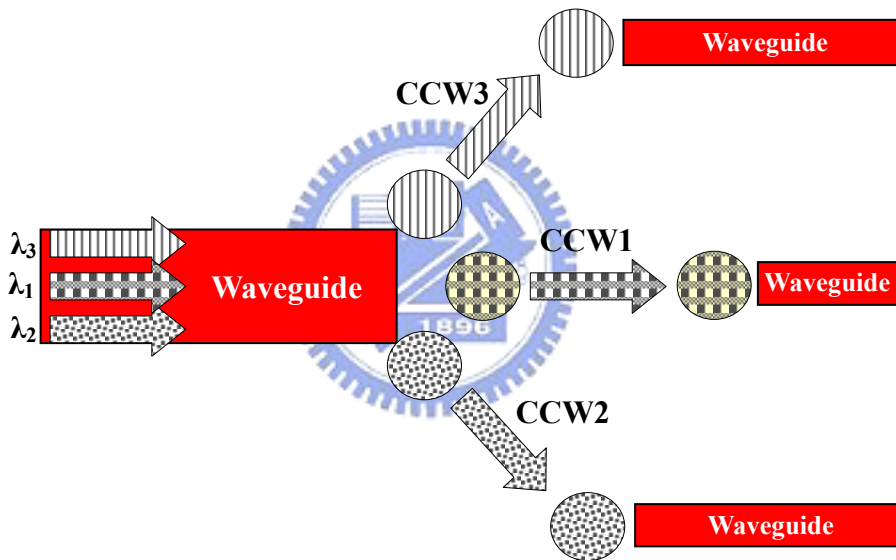


Fig. 3-12. (a) Low Δf and $\frac{\partial \omega}{\partial k}$ of slow light band. (b) Only the resonance frequency (denoted as f_1) can be transited through a CCW.

We try integrating the CCW into the line defect PhC waveguide to complete the WDM design. The structure is made by a 2-D triangular lattice with lattice constant Λ and the material is silicon ($\epsilon = 12$). Silicon rod radius is 0.2Λ , the defect radius is denoted as R_d . In the beginning, we selected the PhC waveguide with $R_d = 0 \Lambda$ to be our primary waveguide. Because of the larger defect band in primary waveguide comparing with the coupled-cavity waveguides, we could slice the guiding mode into piece. In other words, light with multi-frequency guided by a line defect waveguide was separated by running into the coupled-cavity waveguide with different R_d . Such a description is easily sensed in the following Fig. 3-13.



(a)



(b)

Fig. 3-13. (a) Four slow light bands were brought from different coupled-cavity waveguides. (b) Sketch of our WDM idea.

3-2.3 FDTD simulation to photonic crystal WDM

Now we have already recited our design conception above and then are ready to do the further simulation of PhC WDM. In the first step, resonance frequencies of each CCW must be calculated accurately. By using the plane wave expansion method to solve the dispersion

relation of the coupled cavity waveguides, Table 3-3 reveals the resonance frequencies of some similar point defects having varied R_d . In order to match the optical communication wavelengths (1300 nm to 1550nm in usual), lattice constant Λ was quantified as 0.51 μm and 0.57 μm in the following list.

Point defect radius (Λ)	Frequency range (c/Λ)	Central frequency (c/Λ)	Wavelength @ $\Lambda = 0.51 \mu\text{m}$	Wavelength @ $\Lambda = 0.57 \mu\text{m}$
0	0.39247~0.39249	0.392485	1304nm	1456nm
0.025	0.39188~0.39191	0.3919	1306nm	1458nm
0.05	0.38152~0.38153	0.381528	1341nm	1498nm
0.06	0.369861~0.369867	0.369864	1383nm	1545nm
0.065	0.365222~0.365226	0.365224	1401nm	1565nm

Table 3-3. The resonance frequency of each point defects and its corresponding wavelength due to two sizes of lattice constant (Λ).

We chose the normalized frequencies 0.392485 and 0.381528 (i.e. $R_d = 0$ and $R_d = 0.05 \Lambda$) to do the initial test of WDM which can separate 2 wavelengths. After the optimum design, the structure is shown in Fig. 3-14(a). Due to the different ability of localizing waves in reduced and void rod cases (this part has already been well discussed in the last section), the coupling effect of those two systems are not exactly so similar, actually they're quite different. It is too involved a subject to be treated here in detail. On the basis of the reason above, the structures of each frequency become dissimilar. Fig. 3-14(b) and (c) show us the simulation results after we pumping two frequencies into primary waveguide. It is clear to see that two different wavelengths (1304nm and 1341nm in $\Lambda = 0.51 \mu\text{m}$) are successfully separated and guide to their own waveguide.

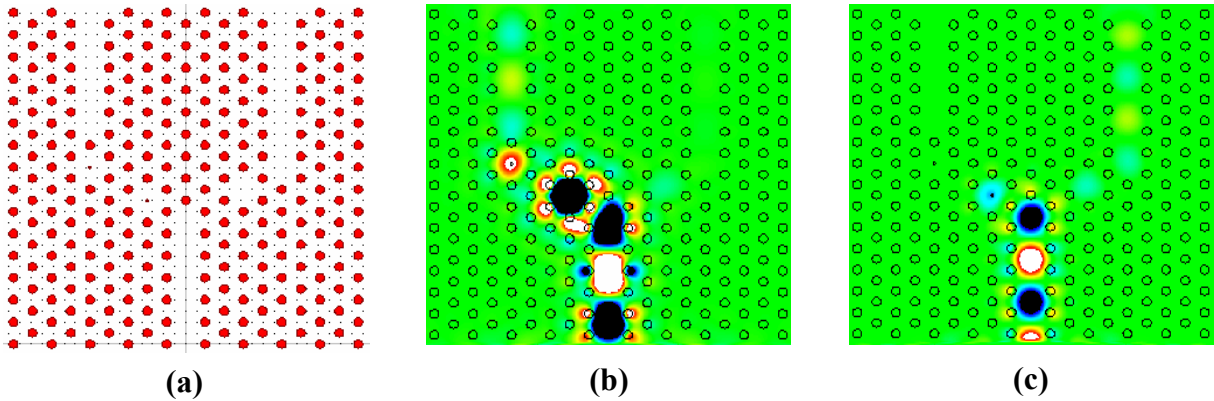


Fig. 3-14. (a) Optimum design by considering the coupling effect of reduced and void rod cases. (b) 1341nm and (c) 1304nm @ $\Lambda = 0.51 \mu\text{m}$.

Let us now look closely at the sample of three wavelengths division multiplexing system. We changed all point defects into reduced rods in the cause of lessening the diversity of each coupling effect and getting a simpler configuration (the part for filter and coupled region, which marked with blue circle in Fig. 3-15). The R_d we chose are 0.025, 0.05 and 0.06 Λ to divide the wavelengths with 1306 nm, 1341 nm and 1383 nm in $\Lambda = 0.51 \mu\text{m}$. The power ratio of random two ports in three wavelengths we mention foregoing can achieve the region between 16.4 dB to 38 dB (consulting the Table 3-4). The corresponding results of FDTD simulation are shown in Fig. 3-16. Even if the power ratios of our design conform to the optical communication standard in most cases, the transmittance of the power passing through the coupled region we marked in Fig. 3-15 is still low with only 10 % or less. This indicates that the large number of energy waste on reflection in primary waveguide.

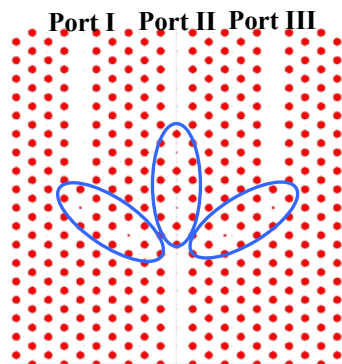


Fig. 3-15. The structure of our second design of PhC WDM. All point defects are formed with reduced rod. We can call this a symmetric design cause its concise composition. Blue circle marks the filter and coupled region in order to separate multi-wavelengths.

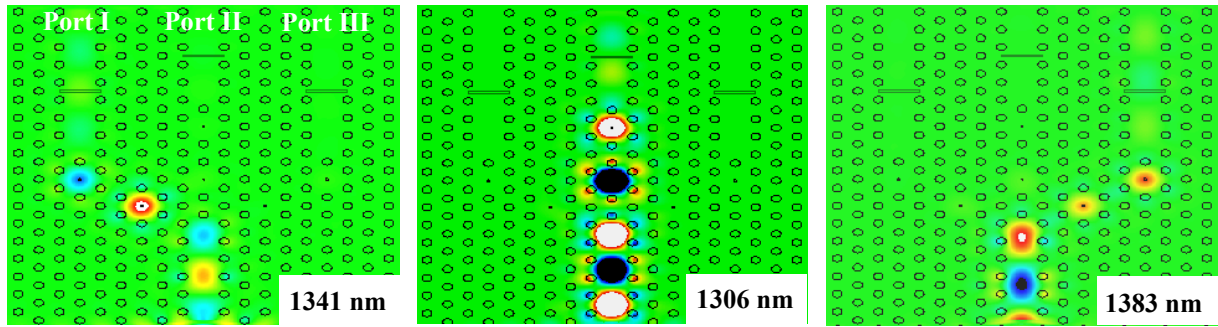


Fig. 3-16. The FDTD simulation to the PhC WDM with $\Lambda = 0.51 \mu\text{m}$ which separates three wavelengths. Large reflection appeared in the input port that led to low transmittance less than 5 %.

Input wavelength ($\Lambda=0.51\mu\text{m}$)	Power ratio (dB)		
	Port I vs Port II	Port I vs Port III	Port II vs Port III
1341 nm	16.4	31.2	--
1306 nm	38	--	32
1383 nm	--	23.8	20.3

Table 3-4. Output power ratio of WDM in our second design.

The question now arises: How can we enhance the transmittance to avoid energy loss? The answer may be found in the boundary of coupling region and the photonic crystal waveguide. Up to the present, the work function of our WDM design always follows the flow chart as shown in Fig. 3-17(a). Its two boundaries between coupled region and usual photonic crystal waveguide are the most important reason of low transmittance. Since the different behavior of a resonator and waveguide, a signal might be easily trapped by the coupled region but it's pretty hard to well coupling to the photonic crystal waveguide in the output port. This problem is necessary for us to solve. The only way I can imagine is trying to improve the coupling effect in second boundary (i.e. coupled region\output port). We can make good use of coupled-cavity waveguide (CCW) which we have discussed in section 3-1.4. With the same

basis, they are all constructed by inducing several point defects, the boundary influence might be reduced. To prove this argument, we change the photonic crystal waveguide in the output port into a coupled-cavity waveguide which is formed by placing point defects side by side with a periodicity of 2Λ and then put it into FDTD simulator. The size of the point defect in CCW is the same with that of its own coupled region in each port. Fig. 3-17(b) shows the flow chart of this improved work function of the third design of DWM.

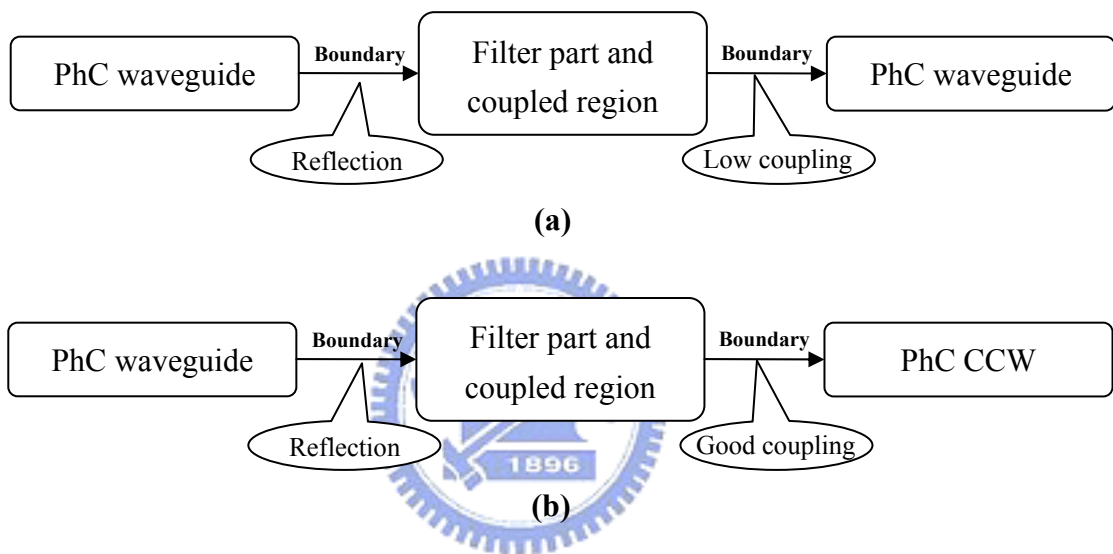


Fig. 3-17. The flow charts of our two WDM work functions. (a) Low transmittance is produced from the disadvantageous boundary effect. (b) Improving the coupling efficiency of the second boundary by inducing a CCW.

After the redevelopment in output waveguides, the transmittance efficiency does really increase a lot. In the case of 1306 nm, 1341 nm and 1401 nm (where $\Lambda = 0.51 \mu\text{m}$) their transmittance is up to 21%, 90% and 16% respectively. The field pattern can help to see that distinct change (Fig. 3-18). The power ratio has also been taken down on Table 3-5.

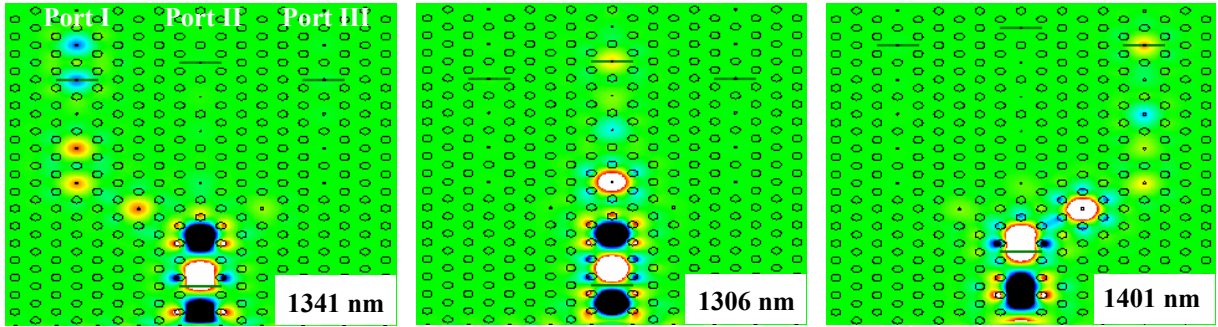


Fig. 3-18. Our third design of PhC WDM. We replaced the output waveguide into CCW and that will help reducing the energy loss. Where the thin rectangles are the monitor which output the data during the FDTD simulation. Λ is $0.51 \mu\text{m}$.

Input wavelength ($\Lambda=0.51\mu\text{m}$)	Power ratio (dB)		
	Port I vs Port II	Port I vs Port III	Port II vs Port III
1341 nm	31	20.7	--
1306 nm	23.8	--	25
1401 nm	--	23.4	43

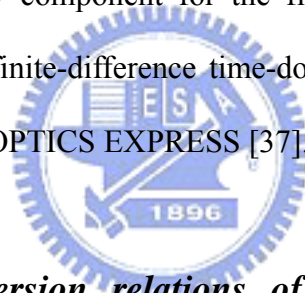
Table 3-5. Output power ratio of the third WDM design.

3-2.4 Summary

Wavelength division multiplexing (WDM) is indispensable in communication industry nowadays. However, it is still keeping in the scale of centimeters in the present. That makes the goal of optical integrated circuit becoming hard to achieve. On the other hand, the main advantage of photonic crystal WDM is its ability of reducing the device's scale to micrometer and realizes the "on-chip" prospect. In addition, according to our analysis above, we can find it's easy to obtain a satisfied power ratio if the point defect is applied. Several wavelengths can be successfully separated by using the slow-light band property of point defect in our WDM design with small size (only few micrometers). We believe that can be a useful idea of the future on-chip WDM design.

3-3 Dual wavelength demultiplexing by coupling and decoupling of photonic crystal waveguides

Recently, the power transfer properties of parallel coupled PCWs have been studied and devices such as directional couplers, switches, and multiplexers/demultiplexers have been proposed using the waveguide coupling. It indicates that there exists a large potential in designing various compact photonic devices by using the large dispersion of coupled mode splitting. In the following analysis, we apply a particular phenomenon which called “band-crossing” in PCWs to the design we present in the follow. By employing the “decoupling” at the frequency of crossing-point, we designed a dual-wavelength demultiplexer, which is a key component for the fiber-to-the-home optical network. The simulation is verified by the finite-difference time-domain (FDTD) method and this article has already been published in OPTICS EXPRESS [37].



3-3.1 Study to the dispersion relations of two parallel photonic crystal waveguides

The behavior of dispersion relation along the Γ -X direction in single waveguide case has been introduced earlier in Table 3-1. When two waveguides are placed in close vicinity, the crosstalk appears because of the coupling effect and that will make a change in their defect mode. Above all, we do a calculation of the samples we made by placing two PCWs parallel to each other with 1Λ spacing by using plane wave expansion (PWE) method. Instead of the anti-crossing we thought at first, crossing dispersion arose when the electric field pattern was studied. Hence, we found it is not always true that the fundamental mode must be of even parity. Without “adding new pillars at the center of the intra-core region” to generate

“dispersion relations intersect” (this was claimed in Ref. 20), we do demonstrate the fundamental mode of the coupled PCWs can be odd parity in the triangular photonic crystal and the dispersion curves of the coupled PCWs intersect (Fig. 3-19).

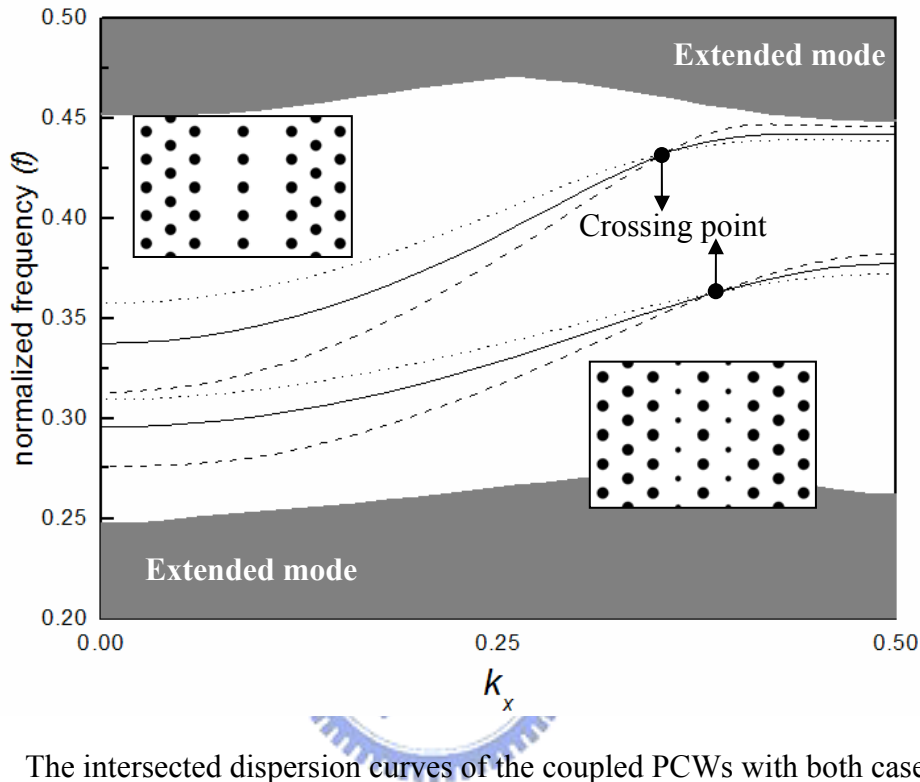


Fig. 3-19. The intersected dispersion curves of the coupled PCWs with both case of $R_d = 0$ and 0.1Λ (R_d represents defect radius). Where the solid lines are the defect mode of single PCW, and the dot and dish lines represent even and odd mode.

3-3.2 Coupling and decoupling of PCWs

A two-dimensional (2D) PhC consists of a triangular lattice of dielectric rods with the lattice constant Λ in air. The diameter and the dielectric constant of the rods are 0.4Λ and 12 respectively. To form a PCW a linear defect of void rods is introduced into a perfect PhC. The extended modes and the defect modes of the TM-polarization (the electric field parallels the rod axis) along the Γ -X direction are calculated. The bandgap ranges from the normalized frequency (f) 0.26 through 0.45 and the defect lie within the bandgap. The linear defect PCW

can be regarded as a chain of point defects, and the defect mode is derived from the superposition of the longitudinal shifted eigenmodes of each individual point defect. As we discussed in section 3-1.4, the dispersion of a linear defect PCW is well fitted by

$$f = \Omega[1 + \kappa \cos(k_x \Lambda)], \quad (3.2)$$

from the tight-binding (TB) approximation, where Ω is the eigenfrequency of a single point defect and κ is the coupling coefficient. In Eq. (3.2), only the coupling of the nearest neighbor defects is taken into account.

When two parallel identical PCWs are brought close enough to have the defect modes well coupled, the defect modes will split into two eigenmodes. The smaller the separation of waveguides, the larger the coupling and the more splitting occurs in dispersion of the eigenmodes. Since a stronger coupling leads to a shorter coupling length, implying a shorter device, here we take the separation of two parallel PCWs (denoted as I and II) as 1Λ . The dispersion relations are shown in Fig. 3-20(a). From the mode patterns calculated by PWE, the eigenmodes appear to be an even parity and an odd parity (Fig. 3-20(b)). Unlike the traditional index-guiding waveguide, the odd mode mainly has an eigenfrequency lower than the even mode, since in this case the effective index of refraction at the guiding region of the PCW is lower than the index of the adjacent PhC. These two modes are degenerate at the point A ($k_x = 0.353, f_A = 0.432$).

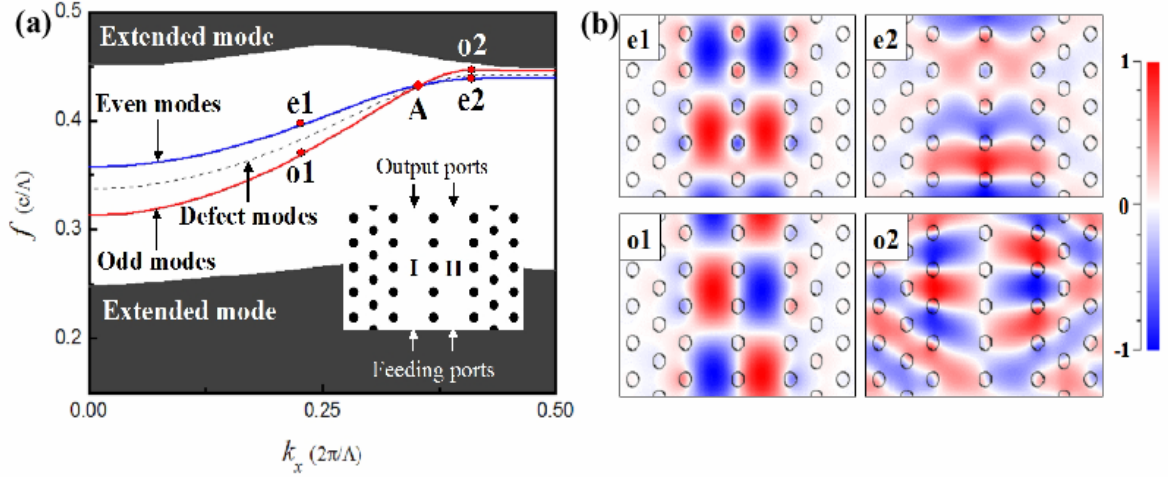


Fig. 3-20. (a) The energy band structures of the extended modes and defect modes of two coupled linear PCWs (I and II). The defect modes of the coupled PCWs are split into two eigenmodes, which cross at point A. (b) The electric field patterns appear as even parity at the points of e1 and e2, and odd parity at o1 and o2. The poor confinement of the electric field at point o2 is a result of being close to the band edge.

Coupling length L can be well described by the eigenmodes expansion [20, 32] and be written as

$$L = \frac{\Lambda}{2\Delta k}, \quad (3.3)$$

where $\Delta k = (k_1 - k_2)$, and k_1 and k_2 are the normalized wavevectors of the even and odd modes at a given f . The analytic dispersion relations of even and odd modes (denoted as f_{even} and f_{odd}) can be separately obtained by fitting with Eq. (3.2) as follow:

$$\begin{cases} f_{\text{even}} = 0.40215 - 0.04463 \cos(k_x \Lambda) - 0.0018 \cos(2k_x \Lambda) + \dots \\ f_{\text{odd}} = 0.38591 - 0.07899 \cos(k_x \Lambda) - 0.00602 \cos(2k_x \Lambda) + \dots \end{cases} \quad (3.4)$$

After neglecting the coupling of further neighbors, the corresponding k point of both modes

can be estimated by fixing the frequency f .

$$\left\{ \begin{array}{l} k_{even} = \frac{1}{2\pi} \cos^{-1}\left(\frac{0.40215 - f}{0.04463}\right) \\ k_{odd} = \frac{1}{2\pi} \cos^{-1}\left(\frac{0.38591 - f}{0.07899}\right) \end{array} \right. \quad (3.5)$$

To ignore the minus and positive sign before the number, Δk can be calculated by taking the modulus to $(k_{even} - k_{odd})$, thus L as the function of f can be plotted as shown in Fig. 3-21(a). The value of L varies dramatically from 2.5Λ to infinity for the coupled PCWs. Infinite L occurs at point A, attributed to the degeneracy of the eigenmodes and the fact that $\Delta k = 0$. The real-time evolution of the optical waves in the coupled PCWs is simulated by the FDTD method (Fig. 3-21(b) and (c)). If one launches a Gaussian wave with a width of $\sqrt{3}/2 \Lambda$ at frequency $f_A = 0.432$ in the PCW I, then both eigenmodes will be excited. The optical wave keeps traveling without transferring into PCW II, even though its field extends over the PCW II. Hence, the two PCWs are decoupled at point A. Here we called “decoupling” does not imply “no coupling” existing between the PCWs. In fact, those PCWs are still coupled at point A, but their two eigenmodes propagate at the same wavevector with no beating between the modes.

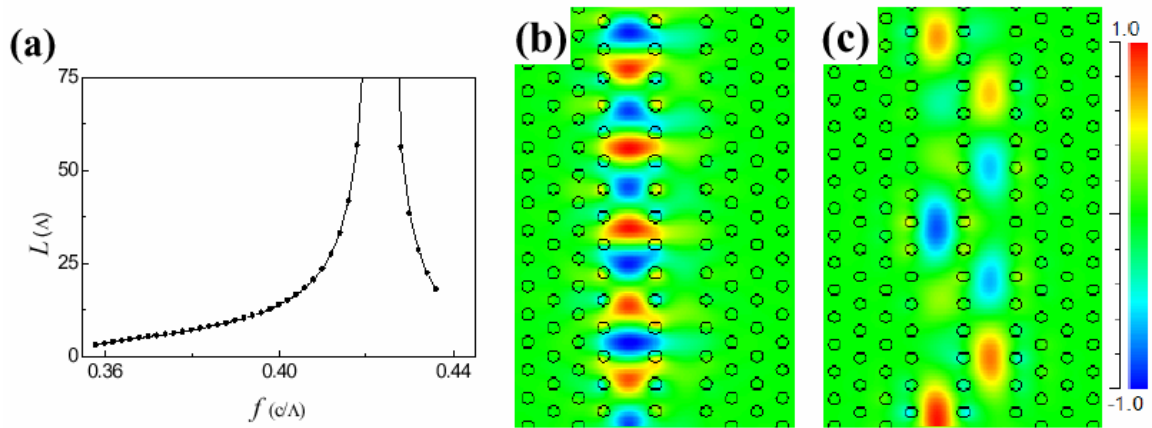
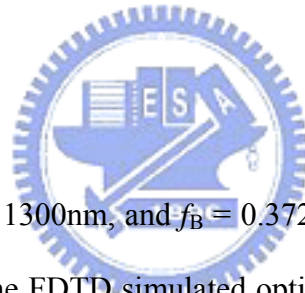


Fig. 3-21. (a) The plot of the coupling length L as the function of frequency f . L varies rapidly near crossing point (L over 75Λ is not shown). FDTD simulated electric field of the coupled PCWs at f_A (b) and $f_B (= 0.372)$ (c) fed into PCW I. The coupling length of f_A is near infinite and that of f_B is 4.6Λ .

3-3.3 Demultiplexing



Let f_A correspond to $\lambda_A = 1300\text{nm}$, and $f_B = 0.372$ for $\lambda_B = 1500\text{nm}$ if $\Lambda = 0.56 \mu\text{m}$ thus $L_B = 4.6 \Lambda$ and $\Delta k = 0.108$. The FDTD simulated optical wave of f_B transfers back and forth periodically between the two PCWs, because of beating of the eigenmodes (Fig. 3-21(c)). Due to the distinction of coupling and decoupling, the waves of f_A and f_B therefore would be demultiplexed. Our preliminary demultiplexer design is shown in Fig. 3-22. Two feeding PCWs are separated by five rows of rods to prevent the channel crosstalk, and the coupling region is 4Λ long with one row separation. Clearly, the wave of f_A propagates only in PCW I without power transferring, and the wave of f_B completely transfers to the PCW II through the coupling region. The output power ratio (P_1/P_2) of f_A is 26 dB (Table 3-6). However, the ratio of f_B is only 10.7 dB, since the wave propagates in both forward and backward directions in PCW II. It is not so simple to enhance the efficiency of Demux I if the feeding port of PCW II was removed. As Fig. 3-22(c) shows, the wave is bounced off the PCW II back to PCW I and

the demultiplexing is destroyed.

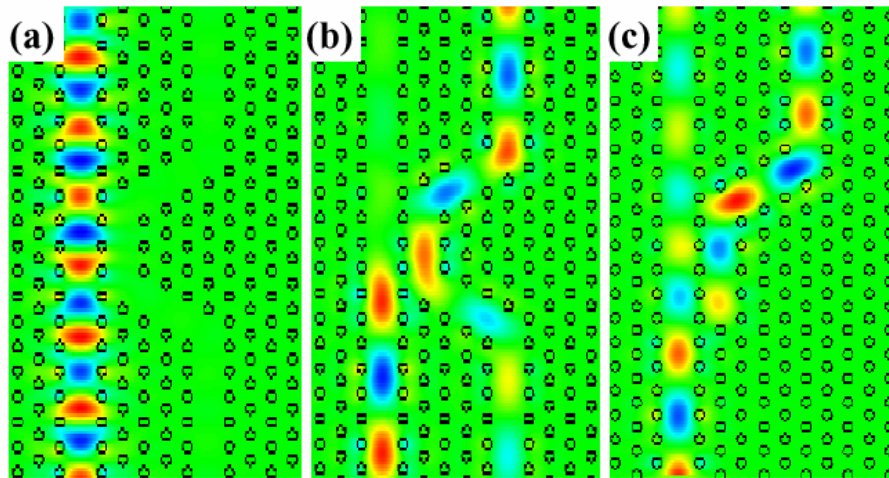


Fig. 3-22. FDTD simulated electric field maps of coupled PCWs; a bar state for f_A (a) and cross state for f_B (b), while both forward and backward couplings happen to f_B . As the feeding port of PCW II is removed (c), the wave of f_B transfers back to PCW I.

Table 3-6. Output power ratios of demultiplexers*

	Demux I		Demux II
	P_1/P_2 (dB)	P_1/P_3 (dB)	P_1/P_2 (dB)
f_A	26	26	15.6
f_B	10.7	6	16.2

* $f_A = 0.432, f_B = 0.372$. P_1 is the power at the desired output port, P_2 the residue power at the other output port, and P_3 the backward power of PCW II.

3-3.4 The feed back design: A hexagonal loop

In the burn-in test of electric industry, there exists a burn-in test system called “LoadSaver” or “Energy recycling system” (Fig. 3-23(a)) [38-40]. The LoadSaver combines versatility while significantly reducing the energy cost of testing high power sources. It saves on installation because of the lower current feed and lower cooling requirements. Fig. 3-23(b) shows a typical LoadSaver configuration, with 10 kW drawn from the sources under test. If these sources are 90% efficient, 11kW will be drawn from the mains. However due to the

recycling abilities of LoadSaver, 8.5 kW of this power shall be returned to the mains resulting in a net power draw of 2.5 kW for the total system. The above-mentioned is not so interesting for us because of the key point we noticed is only in the end of that feedback loop (we marked with point X). In an AC electric power system, if the phase of the feedback current (3 phase in usual) does not match to that of the main current, the electric pollution will occur and that might cause great damages in the whole electric network. Thus, above principle provided an ideal for us to design a photon feedback loop for reducing the photon leakage. Such can also be called as a photon recycling circuit.

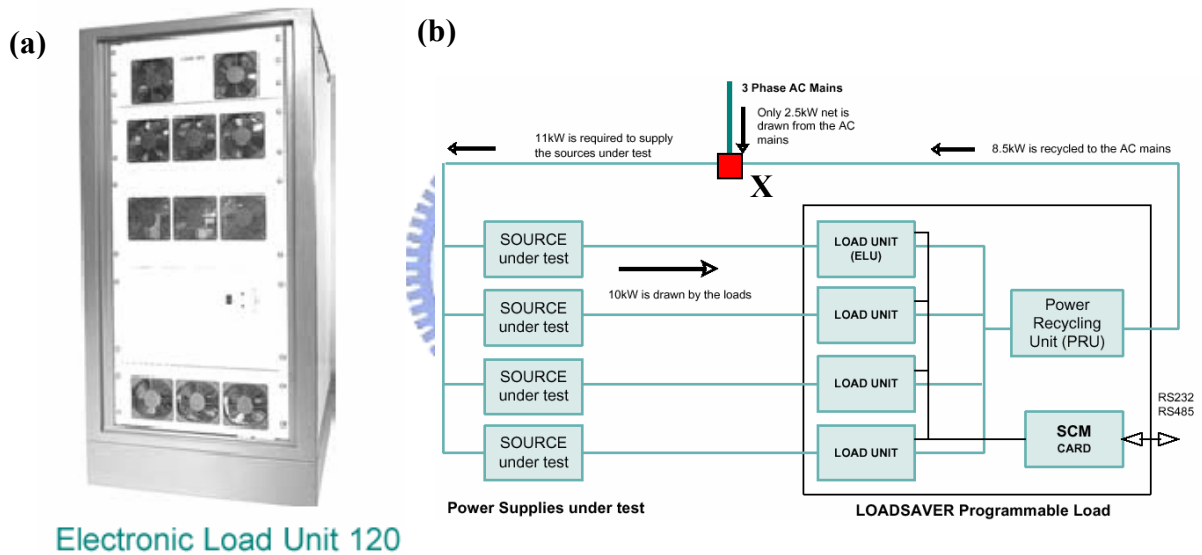


Fig. 3-23. The LoadSaver produced by SCHAFFNER (a) and its typical configuration (b). To avoid the electric pollution in the whole power network, the phase of the feedback power must be matched to the mains in the point we denoted as X.

We therefore propose a novel design (denoted as Demux II) to deal with the backward coupling. Instead of removing the feeding port of PCW II, we make it a hexagonal loop with the coupling length of 5Λ , as shown in Fig. 3-24. The backward coupled wave can merge with the forward wave after traveling the loop. In-phase or constructive interference of the

forward and backward waves at the merging point is crucial for maximum output power. If there is a phase mismatch, part of the coupled wave will transfer back to PCW I. The interference can be turned by changing the shape or size of the loop. The optimum design in Fig. 3-24(a) is to make the hexagonal loop three rows in width and five rows in length, so that the interference is constructive. The output power ratio of f_B is increased to 16.2 dB as the backward wave is eliminated (Table 3-6). The inevitable penalty is the output power ratio of f_A decreases to 15.6 dB, which is comparable to the previous result. Some changes in either width or length of the loop will shift the constructive interference and decrease the output power ratio, as shown in Fig. 3-24(b).

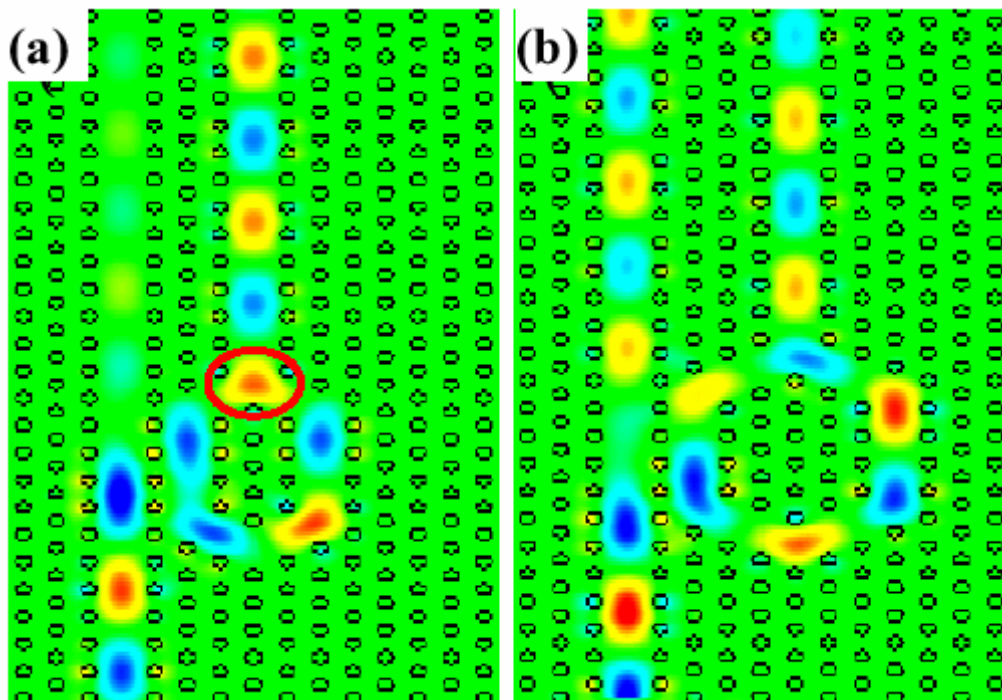


Fig. 3-24. (a) The loop layout applied to the PCW II for eliminating the backward coupling. The coupled forward and backward waves are in phase at the merging point (marked with the red circle). (b) The coupling efficiency decreases, as the waves are not in phase at the merging point. The frequency is f_B .

3-3.5 Other discussion

We test the demultiplexing bandwidth by injecting an optical wave deviated from the nominal frequencies with FDTD simulation. The available bandwidth ($\Delta f/f$) around f_B is about 5%. That is enough to cover the bandwidth of typical laser diodes employed in optical communication network. The demultiplexer operated near f_A appears with a much wider bandwidth, because the coupling length is much longer than the coupling region. Hence the influence of coupling length variation can be ignored. The channel with larger bandwidth can be used to carry more information during the data transfer. It is similar to the spectrum division of ADSL (Asymmetric Digital Subscriber Line) nowadays (Fig. 3-25).

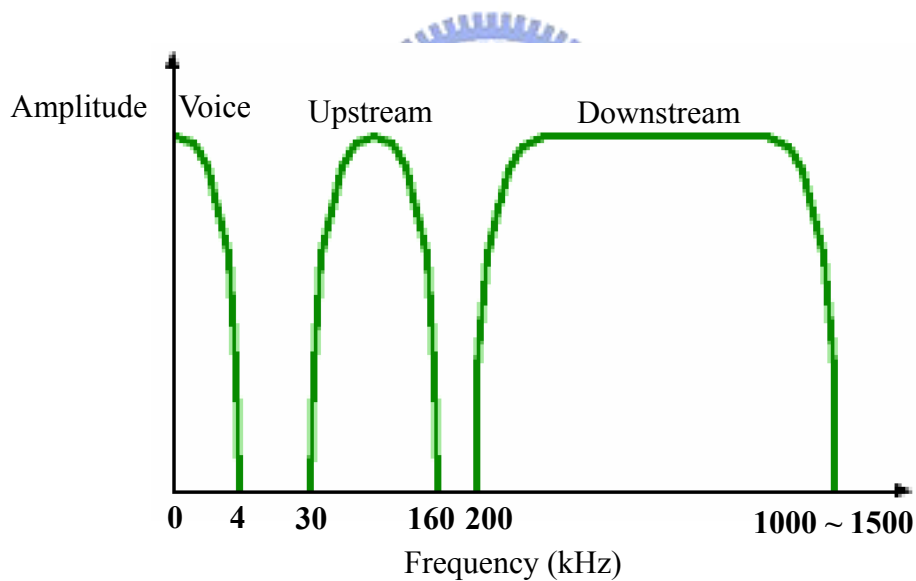


Fig. 3-25. The frequency spectrum of the ADSL which is operated base on 2 pairs of copper wires. Large downstream bandwidth is due to the high data rate requirement in the user terminal.

3-3.6 Summary

For the extremely large splitting ($\Delta k = 0.108$) of the coupled PCWs, a coupling length of only 4.6Λ is required for total transfer of power. In our design, the coupling region is 5Λ (equal to two wavelengths). However, it is still rather tiny compared with traditional coupling devices of millimeter scale.

Without adding new rods at the center of the intra-waveguide region, we demonstrated the fundamental mode of the coupled PCWs can be odd parity in the triangular photonic crystal and the dispersion curves of the coupled PCWs do intersect. Thus, the PCWs are decoupled at the crossing point. By employing the decoupling at the crossing-point at wavelength of $1.3 \mu\text{m}$ and ultra short coupling length of 5 lattice constants at $1.55 \mu\text{m}$, we designed a dual-wavelength demultiplexer with output power as high as 15 dB. A loop-shape PCW is proposed to increase the demultiplexing efficiency. A constructive interference at the merging point of the loop is necessary to have the maximum power transfer. We believe the performance, for example, output power ratios, can be further improved by fine tune of the geometrical features.

3-4. Design of an optical bidirectional module with coupled photonic crystal waveguides

As we talked in section 3-3, here we also take advantage of the coupling and decoupling of the photonic crystal waveguides to do our following bidirectional communicator design. By choosing the frequency at the crossing point, we can have a “reversible” bidirectional coupler (i.e., it can be used in both server and user terminal). The dispersion relations are calculated by PWE and the numerical experiment is verified by FDTD method.

3-4.1 Introduction to optical bidirectional multiplexer

Bidirectional optical multiplexer is a common element in fiber optic networks. The appeal of bidirectional transmission is that in many cases only one fiber would be necessary, thus reducing the cost of installing metro networks (Fig. 3-26). Bidirectional transmission requires an emitter/Tx (laser diode; LD) and detector/Rx (photon diode; PD) at each end of the fiber. An emitter and detector can be the same device, and switching by the forward and reverse bias (electrical) or the waveguide splitters (optical). Other devices like bidirectional add/drop amplifier (BADA) [41] and optical interlinking [42] have already been widely studied.

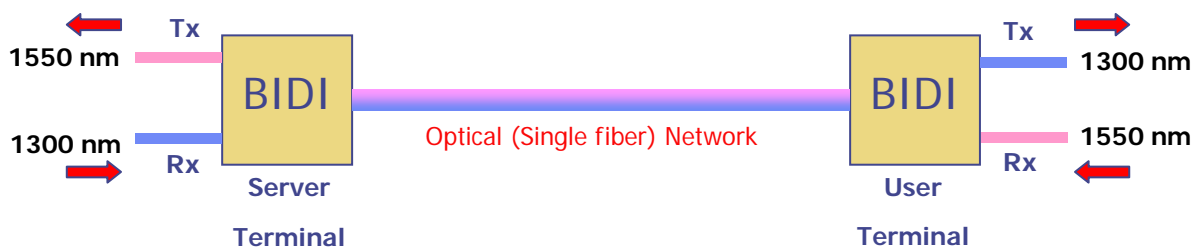


Fig. 3-26. Typical work function of optical communication network and the role of the bidirectional (BIDI) multiplexer.

Due to the centimeters (cm) scale of the bidirectional multiplexer nowadays (Fig. 3-27), we expect to reduce the size to only several micrometers. By taking good use of photonic crystals, small size and on-chip manufacture can be easily achieved; others like transmission loss can also be well controlled.

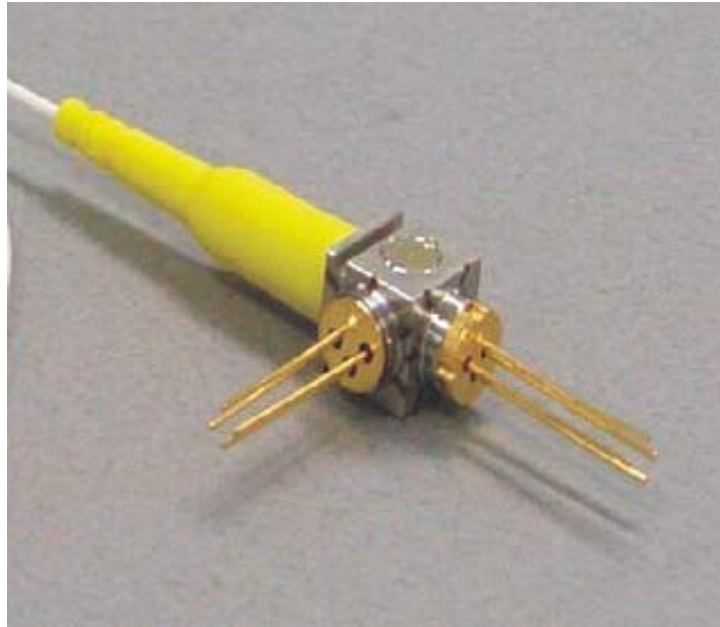


Fig. 3-27. Bi-Direction optical front-end (1310nm LD/1550nm PD) which is made by **Asia-optical**. The emitter is MQW FP or DFB laser, and the detector is InGaAs/InP PIN photodiode.

3-4.2 The structure of our PhC bidirectional module

The structure of our photonic crystal waveguide is made by introducing reduced rods ($R_d = 0.1 \lambda$) into a perfect triangular photonic crystal with rod radius $R = 0.2 \lambda$. The material is silicon (epsilon = 12) and the background is air. By placing two such waveguides side by side with the spacing only one row of rod, the coupling effect (or crosstalk) is occurred and the dispersion relation (TM-polarization) of such a coupled waveguides system can be calculated

by PWE method as shown in Fig. 3-28a. The solid line is the defect mode of single waveguide. After two waveguides approach to each other, a single defect mode would separate into two bands (even and odd denoted as dot and dish, respectively). This can be clearly described by comparing the field patterns of separated bands in Fig. 3-28b.

To take advantage of the field-localized property in reduced rod PCW, as illustrated in Fig. 3-2, we can easily improve the backward coupling which happened in the earlier design (as shown in Fig. 3-22 in section three). Due to its more obvious cavity-like properties of reduced rod PCW, the energy can be more completely coupled and guided to the neighbor waveguide. Such a thought has been proved by the FDTD simulation in Fig. 3-28c.



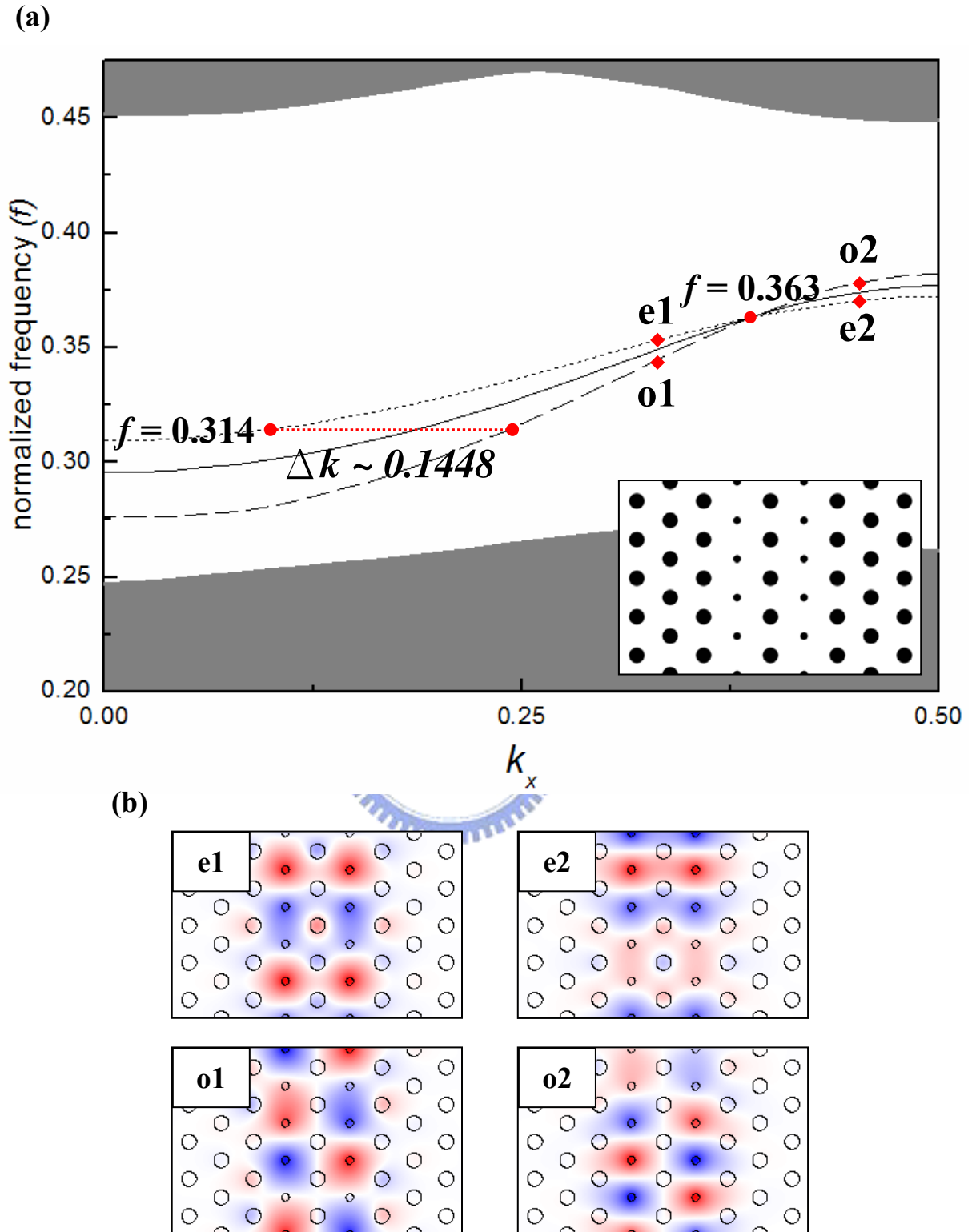


Fig. 3-28. (a) The band separating by two approached PhC waveguides, where the solid, dot and dish denoted as the defect mode of single waveguide, even and odd mode respectively. (b) Field patterns of four points we indicated in (3-28a).

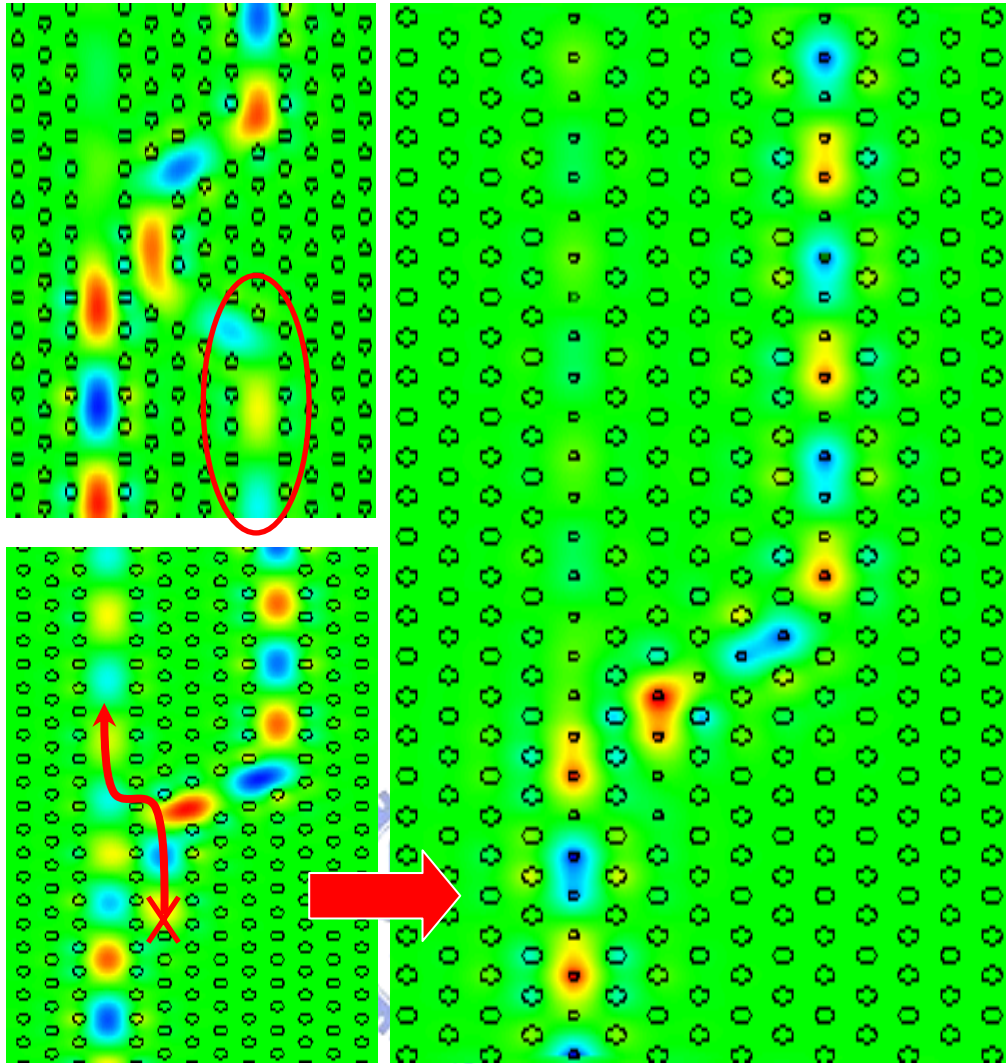


Fig. 3-28. (c) By using the reduced rod PCW, the backward coupling can be high reduced due to its field-localized properties.

As illustrated in Fig. 3-28, the crossing point is at normalized frequency 0.363. If the coupled waveguide system is operated at such frequency, the decoupling effect would come up because of the zero phase mismatch ($\Delta k = 0$) between even mode and odd mode. And we chose normalized frequency 0.314 to be the coupled frequency. We can have the Δk of $f = 0.314$ is 0.1448 (which means the phase difference between two separated modes after traveling one unit lattice). By applying the tight-binding approximation we already mentioned before, we can obtain two curve fitting equations of the even and odd mode in Fig. (3-28a) :

$$\text{Even mode : } f = 0.33909 - 0.0313 \times \cos(k_x \Lambda) \quad (3.6a)$$

$$\text{Odd mode : } f = 0.32283 - 0.05297 \times \cos(k_x \Lambda). \quad (3.6b)$$

Because the coupling length can be written as $L = \frac{1}{2\Delta k}$. Now we can plot the behavior of both Δk and L by using Eqs. (3.6a) and (3.6b), the results are shown in Fig. 3-29.

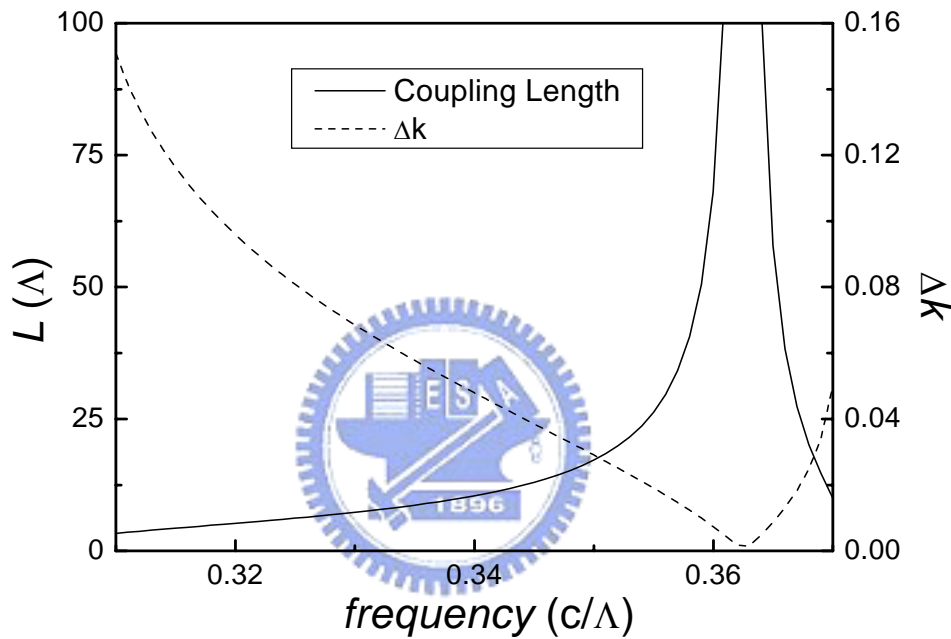


Fig. 3-29. Plot of coupling length L and Δk . We can notice that the decoupling point is at nearly $f = 0.363$, where $L \gg 100 \Lambda$.

The coupling length L of $f = 0.314$ can be found in Fig. 3-29 is about 3.4Λ . After all, we design our optical bidirectional multiplexer as illustrated in Fig. 3-30. Here we no longer use the normalized frequency. In order to match the wavelength range 1300-1550 nm in common optical communications, we defined some structure parameters. The material of our BIDI is still made by silicon but we set our lattice constant as 480 nm, therefore our original and reduced rods diameter becomes 192 nm and 96 nm, respectively. The corresponding

wavelength of normalized frequency 0.314 is 1528 nm, and that of normalized frequency 0.363 is 1322 nm. To have a good coupling efficiency of 1528nm, we made the coupling region long as 1920 nm (i.e. 4Λ).

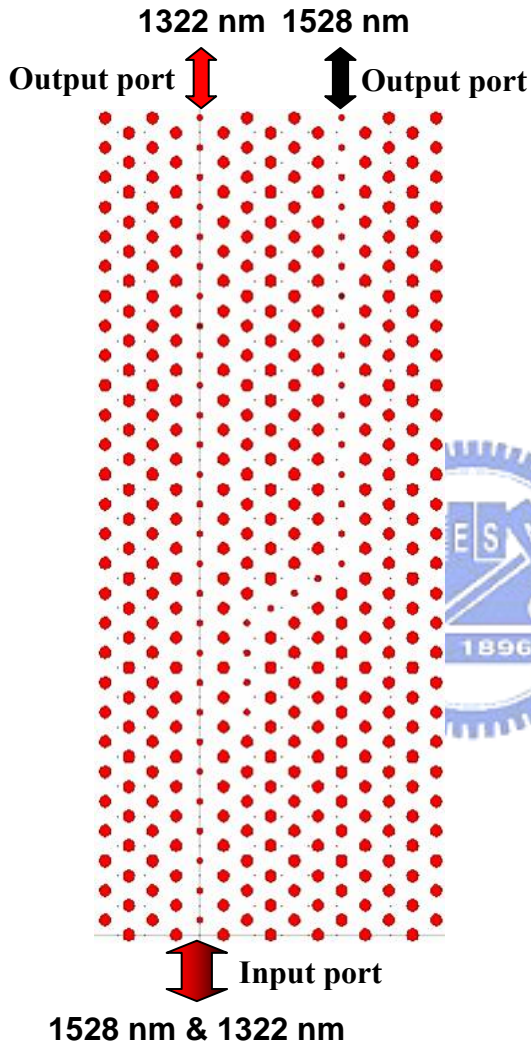


Fig. 3-30. A PhC optical bidirectional module made by silicon rod array. Where $\Lambda = 480$ nm, $R = 96$ nm and $R_d = 48$ nm. By inputting a mixing waves into the input port, they will be separated and guide to the respective waveguides. It can also be treated as a reversible beamsplitter which owns both abilities of optical mixer and demixer.

3-4.3 Simulation and discussion

To confirm our calculation about coupling length L in both wavelengths (1528 nm and 1322 nm), Fig. 3-31 will show the field patterns of light traveling between two close waveguides by FDTD method. In Fig. (3-31a), i.e. 1322 nm case, there exists only few of

power leaking to the neighbor waveguide. That can be taken into a decoupled phenomenon. Differing from the 1322 nm case, with wavelength 1528 nm it has an obvious coupling length about 4Λ due to the power exchange (Fig. 3-31b).

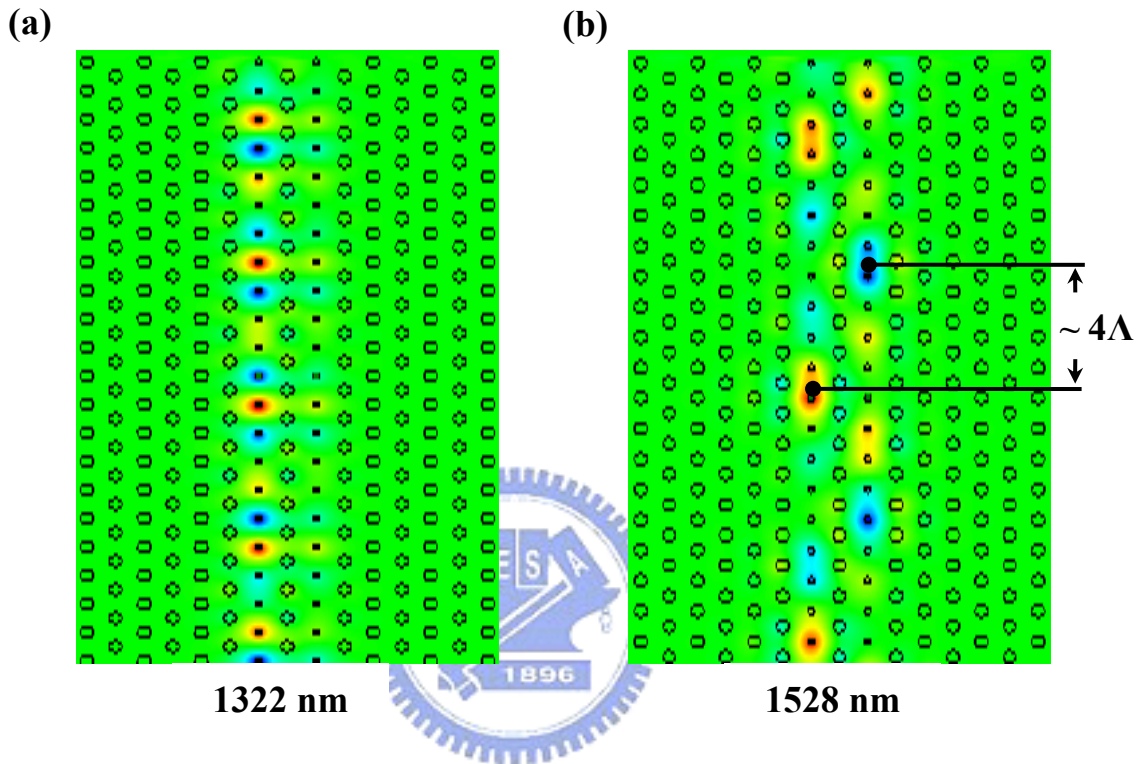


Fig. 3-31. (a) Light traveling along a single waveguide. Only a few power leaks to the neighbor waveguide. That is under a decoupled situation. (b) Because of the modes overlap, the length of power exchange denoted as L is about 4Λ , so called coupling length.

Our BIDI have total three ports in either of two terminals (User and Server). Except the input port, we divided the other two ports into two parts. One is the “desired port”, i.e. the port we wish our signal to be guided to, and another we just called it “other port”. Comparing to the length of the coupling region in our device, any input frequencies with coupling length $L \gg 4\Lambda$ can all be seem to be decoupled. If we therefore define the “decoupled frequency” by the coupling length $L > 100\Lambda$. Then at least we will have an available bandwidth around

$f = 0.363$ in decoupled situations about $\frac{\Delta f}{f} \sim 7\%$. Such a wider bandwidth can be applied to the transmission with large data stream, just like the action of downloading from Server to User end. So we will use the decoupled frequencies (0.363) to carry the signals from Server terminal to User. Oppositely, the frequency $f = 0.314$ which has a narrower bandwidth will do the job of uploading the commands from User terminal to Server.

By placing a time monitor inside our FDTD simulation, we obtained the coupling efficiency $P_{input} / P_{desired}$ in $\lambda = 1528nm$ case is about -1.4 dB. It means almost 72.4% of the power has been completely coupled and guided to the desired port. Another key point is the power ratio between desired port and other port. We have to ensure that the extinction ratio is good enough to be clearly recognized by the photon detector (PD). As shown in Table 3-7, each extinction ratio can all reach to 16.5 dB at least. Such a result makes our design practical. Fig. 3-32(a) shows the transmitting situation of **USER** \rightarrow **SERVER**, and Fig. 3-32(b) is the situation of **SERVER** \rightarrow **USER**. The steady time of each system has also been calculated and written below the figures. They need to take 1.61 to 2.17 *psec* to have a stable transmission.

	T _x	R _x
1322 nm	23.3 dB	17.6 dB
1528 nm	16.5 dB	17.4 dB

Table 3-7 The power ratio of our optical bidirectional multiplexer.

P1/P2; where P1 = desired port and P2 = other port.

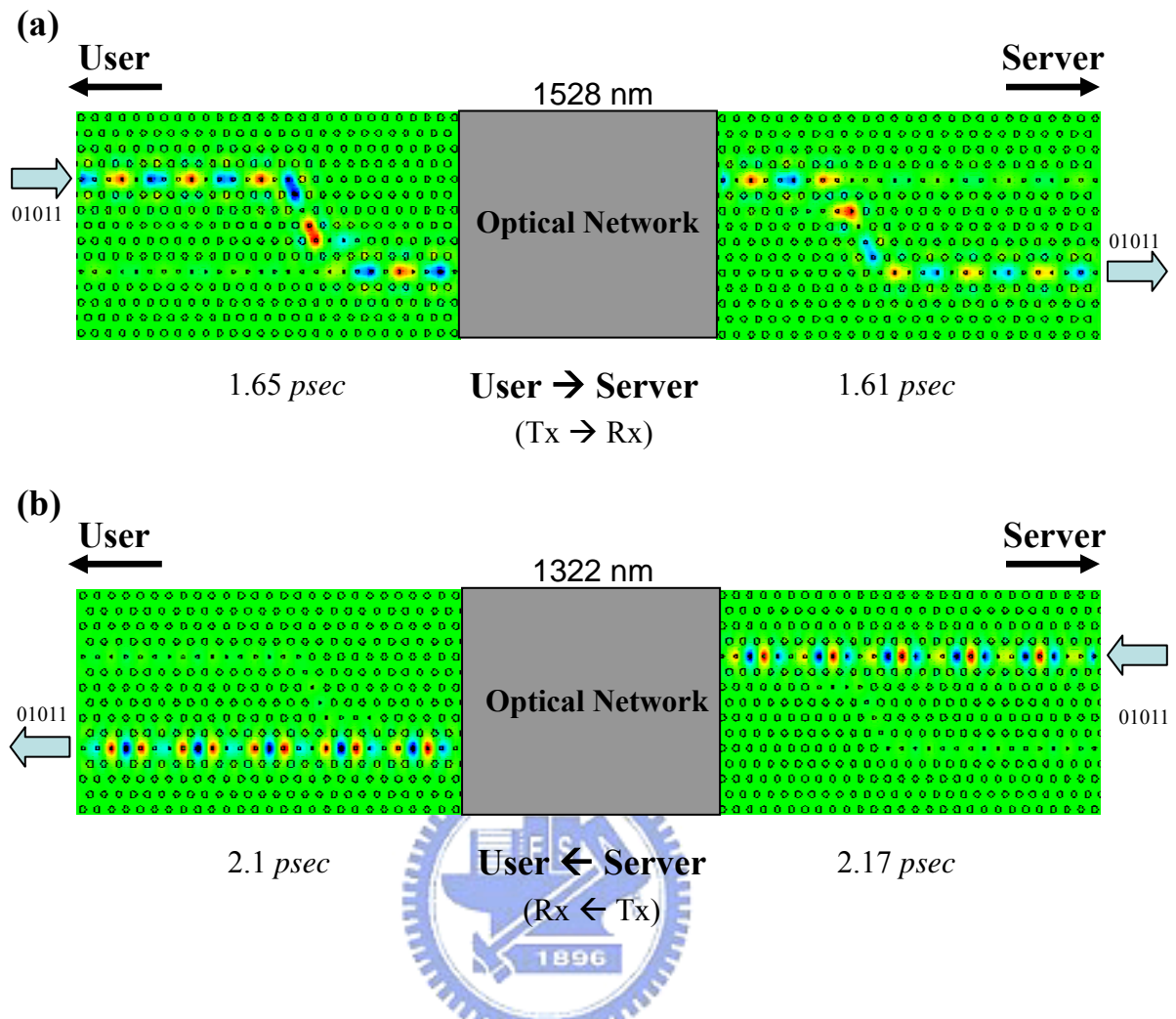


Fig. 3-32. (a) In 1528 nm case, it needs 1.65 and 1.61 *psec* to be steady in Tx and Rx respectively. The coupling efficiency of the coupling region is almost 72.4%. (b) In 1322 nm case, it requires longer time to be steady.

3-4.4 Summary

With applying the reduced rod PhC waveguide, we design a simple structure to achieve the bidirectional transmission. Even if our coupling region is only 1.92 μm (4Λ) length, it can still obtain a good coupling efficiency as high as 72.4% for wavelength 1528 nm. Much smaller than the present bidirectional module, our BIDI has only 12 μm in length and 6.7 μm in width. Hence it is much more advantageous to be an optical inter-linker inside the photonic

integrated circuits (PICs) or the communicator between two chips. By using the same device to be both our Tx and Rx, the manufacturing cost can be reduced. The power ratio of all ports we concerned also seems quite well.

